Chemical Geology 483 (2018) 426–441

Contents lists available at ScienceDirect

Chemical Geology

journal homepage: www.elsevier.com/locate/chemgeo

A noble gas and $^{87}Sr/^{86}Sr$ study in fluids of the Los Azufres geothermal field, Mexico – Assessing impact of exploitation and constraining heat sources

Tao Wen[a,f,*], Daniele L. Pinti[b], M. Clara Castro[a], Aída López-Hernández[c], Chris M. Hall[a], Orfan Shouakar-Stash[d], Fernando Sandoval-Medina[e]

[a] Department of Earth and Environmental Sciences, University of Michigan, Ann Arbor, MI, USA
[b] GEOTOP – Research Center on the dynamics of the Earth System, Université du Québec à Montréal, QC, Canada
[c] Facultad de Ingeniería Civil, UMSNH, Morelia, Mich., Mexico
[d] Isotope Tracer Technologies Inc., Waterloo, ON, Canada
[e] Gerencia de Proyectos Geotermoeléctricos, CFE, Mexico
[f] Now at Earth and Environmental Systems Institute, Penn State University, University Park, PA, USA

ARTICLE INFO

Editor: Dong Hailiang

Keywords:
Geothermal resources
Los Azufres
Helium isotopes
Strontium isotopes
Heat source
Boiling

ABSTRACT

Thirty geothermal wells and two hot springs were sampled for volume fraction and isotopic measurements of noble gases (He, Ne, Ar, Kr, Xe) and strontium in the Los Azufres Geothermal Field (LAGF), Mexico. The aim of this study was to understand the evolution of fluid circulation following three decades of exploitation and re-injection of used brines and to identify the heat source. The LAGF, divided into the Southern Production Zone (SPZ) and the Northern Production Zone (NPZ), is hosted in a Miocene to Pliocene andesitic volcanic complex covered by Quaternary rhyolitic-dacitic units. Air component corrected $^{3}He/^{4}He$ ratios (Rc) normalized to the atmospheric ratio (Ra = 1.384×10^{-6}), range from 4.21 to 7.93 for most samples pointing to the occurrence of a MORB-type mantle helium component, with contributions of crustal helium up to 53% and 18% in NPZ and SPZ, respectively. Observations based on Rc/Ra and $^{87}Sr/^{86}Sr$ ratios point to mixing of three magmatic sources supplying mantle helium to the LAGF: (1) a pure mantle He (Rc/Ra = 8) and Sr ($^{87}Sr/^{86}Sr$ = 0.7035) source related to mafic magmas; (2) a pure mantle helium component (Rc/Ra = 7) with some radiogenic Sr ($^{87}Sr/^{86}Sr$ = 0.7049) source, possibly related to Quaternary rhyolitic magmas; and (3) a fossil mantle He component (Rc/Ra = 4.0) with some radiogenic Sr ($^{87}Sr/^{86}Sr$ = 0.7038), corresponding possibly to Miocene andesitic magmas. Parental magmas related to sources (1) and (2) emplaced < 50 kyrs ago are likely responsible for the addition of mantle volatiles and heat (Q) to the hydrothermal system of Los Azufres. An observed $^{4}He/^{36}Ar$ vs. $^{3}He/Q$ correlation suggests that heat is transferred by conduction and convection in both NPZ and SPZ. Atmospheric noble gas elemental ratios suggest that geothermal wells located closer to the western re-injection zone are dominated by re-injection of used brines (injectate). The area affected by boiling in LAGF has extended further to the north and west since the last noble gas sampling campaign in 2007–2009 (Pinti et al., 2013).

1. Introduction

Mexico is among the countries with the highest installed geothermal capacity in the world (Flores-Espino et al., 2017). The Los Azufres Geothermal Field (LAGF), with an installed capacity of 247.9 MW (Armenta et al., 2016), is the second most productive geothermal field in Mexico after Cerro Prieto (Fig. 1A). LAGF is located 250 km west of Mexico City, in the central area of the Trans-Mexican Volcanic Belt (Fig. 1A). Its geothermal activity is concentrated in a volcanic complex filled with Miocene andesites and covered by Quaternary dacites and rhyolites. The area is part of the Morelia-Acambay east-west rift zone (Fig. 1B) (Ferrari et al., 1991; Torres-Rodriguez et al., 2005). It is a heavily fractured and faulted volcanic hydrothermal system with the geothermal field being divided into the northern production zone (NPZ) and the southern production zone (SPZ). These reflect different geochemical, production and reservoir characteristics. Their original thermodynamic state is also distinct. Indeed, while the NPZ is found solely in the compressed liquid region, the SPZ encompasses the vapor-dominated, liquid-dominated, and compressed-liquid region, depending on the depth (Torres-Rodriguez et al., 2005). The SPZ yields

* Corresponding author at: Earth and Environmental Systems Institute, Pennsylvania State University, 2217 Earth and Engineering Sciences Building, University Park, PA 16802, USA.
E-mail address: jaywen@umich.edu (T. Wen).

https://doi.org/10.1016/j.chemgeo.2018.03.010
Received 7 September 2017; Received in revised form 26 February 2018; Accepted 6 March 2018
Available online 07 March 2018
0009-2541/

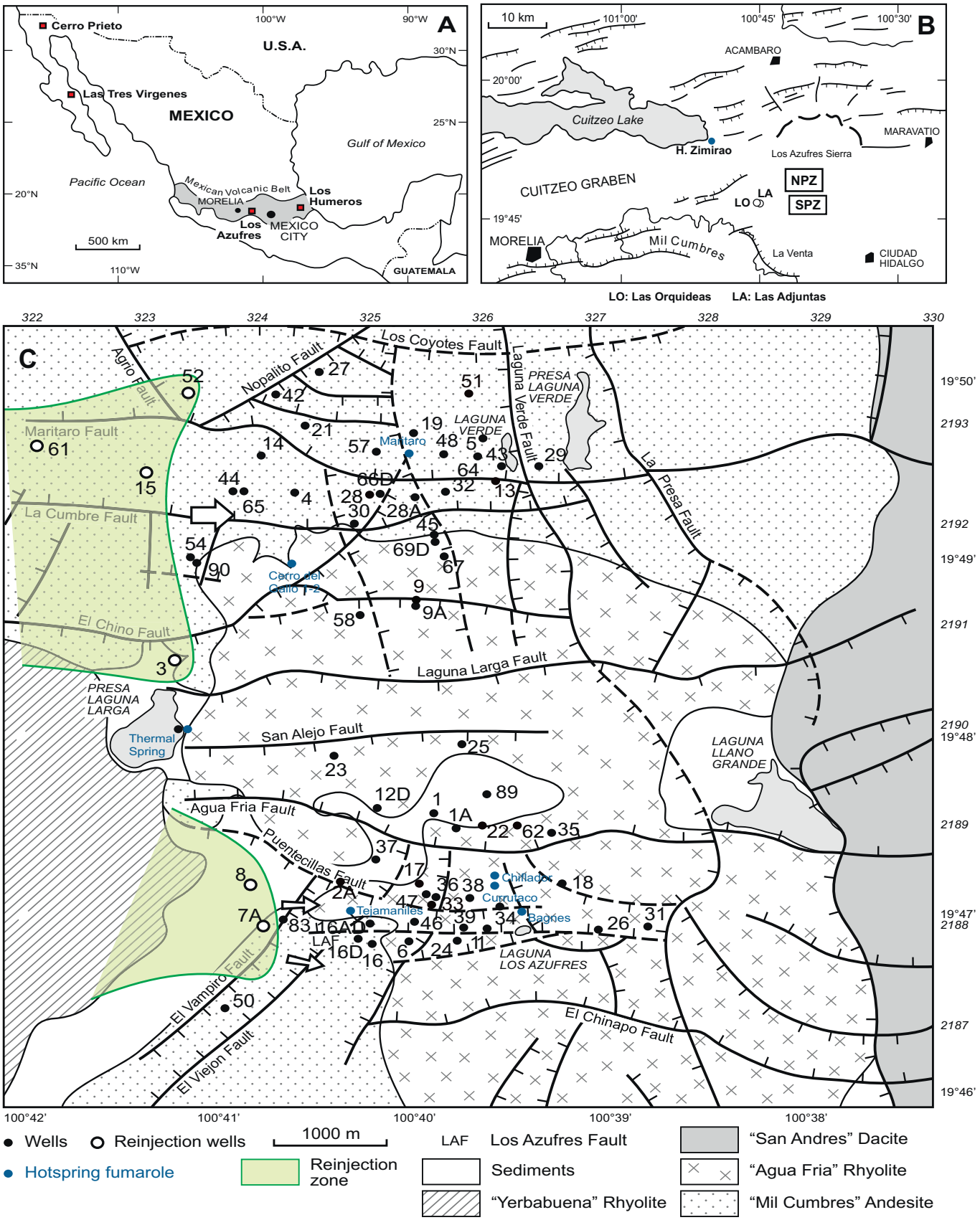

Fig. 1. (A) Simplified map of Mexico with the position of Los Azufres, Cerro Prieto and Los Humeros fields. (B) Simplified tectonic map of the Los Azufres sierra and the E–W rift systems. The location of Araró hot springs on the border of Cuitzeo Lake is also indicated as well as the *H. Zimirao* hot spring. NPZ and SPZ indicate the position of the northern production zone and the southern production zone of Los Azufres geothermal field, respectively (from Pinti et al., 2013). (C) Locations of sampled wells and hot springs sampled in LAGF (this study and Pinti et al., 2013), with tectonic structures and geology. The area of re-injection of used brines (injectate) is reported from Barragán et al. (2005) and Pinti et al. (2013). (For interpretation of the references to colour in this figure legend, the reader is referred to the web version of this article.)

the highest temperatures and is the most productive field.

Since commercial exploitation started at LAGF in 1982, reservoir engineering and geochemical studies were carried out in an attempt to gain knowledge of the reservoir conditions (e.g., Arellano et al., 2015; Garcia-Estrada et al., 2001; Torres-Rodriguez et al., 2005). The fluid chemistry and its evolution as used brine re-injection was also extensively studied (Arellano et al., 2015; Barragán et al., 2005; Birkle et al., 2001; González-Partida et al., 2000, 2005).

Stable noble gases (He, Ne, Ar, Kr, and Xe) are excellent tracers of migration and evolution of subsurface fluids (Castro et al., 1998a, 1998b; Pinti and Marty, 1995; Torgersen et al., 1992; Wen et al., 2015a, 2015b) and have been extensively used to characterize fluids in hydrothermal and geothermal systems (Birkle et al., 2016; Kennedy, 1988; Kennedy et al., 1985, 1991, 2000; Mazor and Truesdell, 1984; Pinti et al., 2017; Saar et al., 2005; Smith and Kennedy, 1985), including at LAGF (Pinti et al., 2013). The study of Pinti et al. (2013) combined noble gases and other geochemical element isotopes (e.g., $\delta^{18}O$, δD, and Sr) and concluded that the NPZ boiling zone had been extended further north following almost 35 years of geothermal fluid exploitation. It further concluded that brine re-injection might account for over 90% of the currently exploited fluids in the westernmost SPZ wells (i.e. AZ-2a; Fig. 1C).

Stable noble gases in geothermal fluids are derived from the atmosphere, the crust, and the mantle, with each of these three terrestrial reservoirs showing distinct isotopic and elemental signatures. This makes it possible to separate each component from the total measured isotopic and elemental abundances. Noble gases of atmospheric origin refer to the component dissolved in water in solubility equilibrium with the atmosphere (Air Saturated Water or ASW). Atmospheric noble gases (ANG) are incorporated into the geothermal system during recharge by meteoric water. Because noble gases have different solubilities, ANG are partitioned in different extents into liquid and vapor phases during boiling and phase separation in the reservoir. Thus, ANG abundance fractionation can be a proxy of the thermodynamic conditions of the reservoir (e.g., Mazor and Truesdell, 1984; Kennedy et al., 2000). Crustal noble gases are primarily produced from radioactive decay of U, Th, and ^{40}K contained in the reservoir rocks (Ozima and Podosek, 1983) and can thus be used to estimate the fluid residence time (Birkle et al., 2016; Pinti et al., 2013). Being prevalent in the mantle and its derived melting products, i.e., the magmas, ^{3}He is ubiquitous in volcanic and hydrothermal areas (e.g., Hilton and Porcelli, 2003; Saar et al., 2005; Sano and Fischer, 2013) while largely absent in the atmosphere (i.e., in meteoric water). Consequently, any fluid having interacted with magmas (either meteoric-derived or “magmatic” from melt crystallization) contains a considerable amount of ^{3}He.

Here, the complete suite of stable noble gases from samples collected in November 2014 at LAGF is analyzed together with previously published data (Pinti et al., 2013). The goal is to further constrain the origin of fluids and heat at LAGF and to assess the impact of physical processes (e.g., boiling, condensation, brine re-injection) on this active geothermal system.

2. Geological background

The general geology of the studied area and the geology of the reservoir at LAGF have been documented in detail in numerous studies (e.g., Dobson and Mahood, 1985; Ferrari et al., 1991; Pradal and Robin, 1994; Torres-Rodriguez et al., 2005) and subsequently summarized by others (Birkle et al., 2001; González-Partida et al., 2000; Pinti et al., 2013).

The Los Azufres geothermal reservoir is hosted in a 2700-m thick fractured, Upper Miocene to Pliocene basaltic andesite to dacite base complex called the *Mil Cumbres andesites* with ages between 18.1 and 5.9 Ma (Dobson and Mahood, 1985). It is overlain by andesitic lavas and basaltic andesites of the *Zinapecuaro andesite* unit dated at 0.87–0.85 Ma. The reservoir is sealed by a silicic sequence of rhyodacites, rhyolites and dacites with ages between 1.6 and 0.15 Ma (Dobson and Mahood, 1985). At least five larger volcanic episodes affected the LAGF in recent geological times: (1) the basal *Aqua Fria rhyolite* dated between 1.6 and 0.84 Ma; (2) the *San Andreas dacite* dated between 0.36 and 0.33 Ma; (3) the *Yerbabuena rhyolite* dated between 0.3 and 0.14 Ma; (4) the *Ciudad Hidalgo basalts* dated approximately at 0.15 Ma; and (5) the last rhyolitic ignimbrite dated between 38 and 26 kyrs (Pradal and Robin, 1994). The felsic sequences of dacites and rhyolites were interrupted at around 0.6 Ma by the emission of numerous lava flows which gave rise to the *La Calabaza* and *Llano Grande* mafic sequences (Pradal and Robin, 1994) (Fig. 1C).

The LAGF is a highly fractured system with faults along the *E*-W, NE-SW and NNW-SSE directions (De la Cruz et al., 1982) (Fig. 1). These faults lead to high hydraulic conductivities along these directions and lead to greater exploitation levels compared to other geothermal fields in Mexico. Fluid temperatures reach values as high as 350 °C with common range values of 240–280 °C (Birkle et al., 2001). The NPZ reservoir consists of the *Mil Cumbres andesites* and *Agua Fría rhyolite* (Torres-Rodriguez et al., 2005). Fluids in the NPZ are in the sub-cooled liquid region (Torres-Rodriguez et al., 2005). The SPZ reservoir has higher temperatures than that of NPZ and is composed of *Mil Cumbres andesites*, *Agua Fría rhyolite* and *Tejamaniles dacite*. The latter is the most recent volcanic unit which hosts most of the thermal springs (Torres-Rodriguez et al., 2005). SPZ fluids are located at three different depth intervals in thermodynamically distinct dominant phases. These are: a) a steam zone at 2300 to 1900 masl; b) a liquid zone at 1900 to 1200 masl; and, c) a compressed-liquid zone at 1200 to 1300 masl. To maintain the reservoir pressure and to increase longevity of the field, re-injection of exploited brines is done at the western border of the NPZ and SPZ productive zones (Fig. 1C). *Re*-injection of brines causes boiling and steam separation in the reservoir (Arellano et al., 2015; Barragán et al., 2005).

3. Sampling and methods

A sampling campaign was carried out in November 2014. Thirty-two gas samples were collected from 30 production wells and 2 springs (Fig. 1C) for analysis of noble gas volume fractions and isotopic ratios (Table 1). Of the two springs, *Maritaro* is located inside the NPZ. The *Hervideros de Zimirao* hot spring (labeled as H. Zimirao; Fig. 1B) was collected nearby the *Araró* locality, a low-medium enthalpy system outside of the Los Azufres sierra (Fig. 1B) (Viggiano-Guerra and Gutiérrez-Negrín, 2005).

Samples for noble gas analyses were collected in standard refrigeration-grade 3/8″ copper tubes (~14 cm^3), sealed by stainless steel pinch-off clamps after gas was flowed through for several minutes. In wells not equipped with a steam/water separator, gas samples were collected directly at the wellhead, using a mini-separator and a cooling coil. In wells equipped with a steam/water separator, the copper tube was fixed to a small stool aligned with one of the output valves of the steam separator conduit. A single copper tube was extended from the sampler to the NPT-type male connector screwed on the steam conduit valve. The clamps were closed using electric drills. Five copper tubes (AZ-18, AZ-34, AZ-51, AZ-62, and AZ-83) were clamped and divided into 2 segments. Each segment of gas sample was measured individually for noble gas volume fractions and isotopic ratios. All replicated analyses from the same copper tube are listed with the suffix ‘a’ or ‘b’ (Tables 1, 2, and 3).

Noble gas measurements were carried out in the Noble Gas Laboratory at the University of Michigan. He and Ne were sequentially analyzed in a Thermo Scientific Helix SFT mass spectrometer while Ar, Kr, and Xe were sequentially inlet into an ARGUS VI mass spectrometer using a computer-controlled double-head cryo-separator. Extraction, purification, and analysis procedures are described in detail in other publications (Pinti et al., 2017; Wen et al., 2015a, 2017). Elemental abundances of He, Ne, Ar, Kr, and Xe have typical uncertainties of

Table 1
Noble gas volume fractions (by volume), F(i) values and $^{87}Sr/^{86}Sr$ values for Los Azufres fluids.

Sample	Type	Field zone	Depth (m)	Bottom-hole temperature or T_G (°C)[a]	Sampled phase	^{4}He	± 1σ	^{20}Ne	± 1σ	^{36}Ar	± 1σ	^{84}Kr	± 1σ	^{132}Xe	± 1σ	F(^{4}He)
						cm^{3}STP/cm^3[d]										
AZ-2A	Well	SPZ	1300	240.6	Dominant liquid zone	5.33E-06	7.99E-08	–	–	2.62E-05	3.40E-07	–	–	1.81E-08	3.98E-10	1.220
AZ-4	Well	NPZ	1950	274.6	Compressed liquid zone	1.28E-06	1.92E-08	2.29E-08	2.98E-10	9.98E-08	1.30E-09	3.16E-09	4.74E-11	1.71E-10	3.77E-12	77.052
AZ-5	Well	NPZ	1493	252.2	Compressed liquid zone	1.29E-05	1.93E-07	1.67E-08	2.17E-10	8.54E-08	1.11E-09	3.21E-09	4.81E-11	1.93E-10	4.24E-12	905.238
AZ-6	Well	SPZ	2000	276.7	Compressed liquid zone	5.48E-06	8.22E-08	1.50E-07	1.96E-09	2.61E-07	3.39E-09	5.42E-09	8.13E-11	1.97E-10	4.33E-12	125.921
AZ-9A[b]	Well	NPZ	1810	268.3	Compressed liquid zone	8.85E-06	1.33E-07	1.66E-08	2.16E-10	5.93E-08	7.71E-10	1.70E-09	2.54E-11	7.61E-11	1.67E-12	894.184
AZ-9AD[b]	Well	NPZ	1800	267.9	Compressed liquid zone	1.22E-05	1.82E-07	3.37E-09	4.38E-11	1.93E-08	2.51E-10	6.19E-10	9.28E-12	2.83E-11	6.23E-13	3776.816
AZ-12D	Well	SPZ	2250	286.6	Compressed liquid zone	2.91E-06	4.36E-08	1.03E-07	1.35E-09	3.18E-07	4.13E-09	8.90E-09	1.33E-10	4.05E-10	8.90E-12	54.820
AZ-13	Well	NPZ	1219	235.2	Compressed liquid zone	1.59E-05	2.39E-07	6.80E-09	8.84E-11	3.00E-08	3.91E-10	1.07E-09	1.60E-11	5.84E-11	1.28E-12	3180.772
AZ-18a	Well	SPZ	1328	242.3	Dominant liquid zone	1.13E-05	1.69E-07	–	–	6.31E-09	8.20E-11	2.43E-10	3.65E-12	1.09E-11	2.39E-13	10,735.577
AZ-18b	Well	SPZ	1328	242.3	Dominant liquid zone	1.37E-05	2.06E-07	–	–	8.00E-09	1.04E-10	2.69E-10	4.03E-12	1.44E-11	3.16E-13	10,299.439
AZ-19	Well	NPZ	1666	261.4	Compressed liquid zone	6.49E-06	9.74E-08	2.28E-07	2.97E-09	7.59E-07	9.87E-09	2.15E-08	3.22E-10	9.64E-10	2.12E-11	51.306
AZ-25	Well	SPZ	2075	279.8	Compressed liquid zone	5.57E-06	8.35E-08	1.87E-08	2.44E-10	9.37E-08	1.22E-09	3.41E-09	5.11E-11	1.97E-10	4.34E-12	356.478
AZ-26	Well	SPZ	1241	236.7	Dominant liquid zone	9.82E-06	1.47E-07	–	–	7.28E-09	9.46E-11	5.29E-10	7.94E-12	–	–	8088.990
AZ-28	Well	NPZ	1680	262.1	Compressed liquid zone	8.07E-06	1.21E-07	4.22E-08	5.49E-10	1.84E-07	2.39E-09	6.12E-09	9.17E-11	3.19E-10	7.02E-12	263.040
AZ-32	Well	NPZ	1559	255.8	Compressed liquid zone	1.49E-05	2.23E-07	6.26E-09	8.14E-11	2.39E-08	3.11E-10	8.17E-10	1.23E-11	1.39E-10	3.07E-12	3732.250
AZ-34a	Well	SPZ	1273	238.8	Dominant liquid zone	1.17E-05	1.76E-07	–	–	1.05E-08	1.37E-10	3.86E-10	5.79E-12	1.65E-11	3.63E-13	6683.144
AZ-34b	Well	SPZ	1273	238.8	Dominant liquid zone	1.37E-05	2.05E-07	–	–	1.14E-08	1.49E-10	4.52E-10	6.78E-12	–	–	7159.067
AZ-36	Well	SPZ	1050	222.6	Dominant liquid zone	1.08E-05	1.62E-07	1.11E-08	1.44E-10	3.30E-08	4.29E-10	9.63E-10	1.44E-11	4.48E-11	9.85E-13	1962.919
AZ-38	Well	SPZ	752	194.6	Dominant steam zone	9.03E-06	1.36E-07	1.78E-08	2.32E-10	4.72E-08	6.14E-10	1.29E-09	1.93E-11	5.77E-11	1.27E-12	1147.432
AZ-42	Well	NPZ	1814	268.5	Compressed liquid zone	6.36E-06	9.53E-08	1.02E-05	1.32E-07	2.89E-05	3.76E-07	–	–	2.86E-08	6.30E-10	1.317
AZ-43	Well	NPZ	1799	267.8	Compressed liquid zone	2.12E-05	3.18E-07	1.12E-08	1.46E-10	5.33E-08	6.93E-10	2.04E-09	3.05E-11	1.18E-10	2.60E-12	2382.929
AZ-46	Well	SPZ	2000	276.7	Compressed liquid zone	7.10E-06	1.06E-07	1.53E-06	1.98E-08	3.57E-06	4.64E-08	–	–	3.29E-09	7.25E-11	11.925
AZ-47D	Well	SPZ	1520	253.7	Dominant liquid zone	7.31E-06	1.10E-07	1.77E-08	2.30E-10	5.71E-08	7.43E-10	1.73E-09	2.59E-11	7.64E-11	1.68E-12	767.275
AZ-48	Well	NPZ	2693	301.7	Compressed liquid zone	8.92E-06	1.34E-07	4.49E-08	5.84E-10	1.98E-07	2.57E-09	6.98E-09	1.05E-10	4.24E-10	9.33E-12	270.194
AZ-51a	Well	NPZ	1842	269.8	Compressed liquid zone	1.53E-05	2.29E-07	1.34E-08	1.74E-10	7.50E-08	9.74E-10	3.03E-09	4.54E-11	1.89E-10	4.15E-12	1222.060
AZ-51b	Well	NPZ	1842	269.8	Compressed liquid zone	3.22E-05	4.83E-07	3.07E-08	3.99E-10	1.79E-06	2.33E-08	1.03E-08	1.55E-10	–	–	107.753
AZ-62a	Well	SPZ	1550	255.3	Dominant liquid zone	1.28E-05	1.93E-07	3.08E-09	4.01E-11	1.32E-08	1.72E-10	4.52E-10	6.78E-12	1.88E-11	4.13E-13	5816.854
AZ-62b	Well	SPZ	1550	255.3	Dominant liquid zone	1.12E-05	1.68E-07	5.32E-09	6.92E-11	1.29E-08	1.67E-10	4.23E-10	6.35E-12	3.13E-11	6.89E-13	5214.197
AZ-65	Well	NPZ	1810	268.3	Compressed liquid zone	9.63E-06	1.45E-07	4.82E-06	6.26E-08	1.79E-05	2.32E-07	–	–	2.21E-08	4.86E-10	3.230
AZ-66D	Well	NPZ	1773	266.6	Compressed liquid zone	4.62E-06	6.92E-08	–	–	2.63E-05	3.42E-07	–	–	1.88E-08	4.14E-10	1.052
AZ-67	Well	NPZ	1910	272.8	Compressed liquid zone	7.53E-06	1.13E-07	2.98E-08	3.87E-10	1.26E-07	1.64E-09	3.84E-09	5.75E-11	1.95E-10	4.29E-12	357.391
AZ-83a	Well	SPZ	1827	269.1	Compressed liquid zone	4.86E-06	7.29E-08	–	–	1.10E-08	1.43E-10	3.55E-10	5.33E-12	–	–	2653.875
AZ-83b	Well	SPZ	1827	269.1	Compressed liquid zone	5.20E-06	7.81E-08	–	–	–	–	–	–	–	–	–
AZ-89	Well	SPZ	1876	271.3	Compressed liquid zone	3.90E-06	5.85E-08	–	–	6.84E-08	8.89E-10	2.30E-09	3.45E-11	1.38E-10	3.04E-12	341.499
AZ-90	Well	NPZ	2230	285.8	Compressed liquid zone	9.63E-07	1.44E-08	1.15E-06	1.49E-08	2.89E-06	3.76E-08	7.25E-08	1.09E-09	2.92E-09	6.42E-11	1.995
Maritaro 4	Spring	NPZ	–	–	–	2.39E-05	3.58E-07	4.80E-07	6.24E-09	1.88E-06	2.44E-08	6.19E-08	9.28E-10	3.74E-09	8.23E-11	76.122
H. Zimirao	Spring	Cuitzeo lake/ Araro	–	–	–	1.85E-06	2.77E-08	5.12E-06	6.66E-08	1.01E-05	1.31E-07	1.43E-07	2.15E-09	8.86E-09	1.95E-10	1.096
Air[c]	–	–	–	–	–	5.24E-06	–	1.65E-05	–	3.14E-05	–	6.50E-07	–	2.34E-08	–	1.000

Sample	Type	Field zone	Depth (m)	Bottom-hole temperature or T_G (°C)[a]	Sampled phase	± 1σ	F(^{20}Ne)	± 1σ	F(^{84}Kr)	± 1σ	F(^{132}Xe)	± 1σ	$^{87}Sr/^{86}Sr$	± 1σ
AZ-2A	Well	SPZ	1300	240.6	Dominant liquid zone	0.024	–	–	–	–	0.928	0.024	0.703758	0.000004
AZ-4	Well	NPZ	1950	274.6	Compressed liquid zone	1.529	0.438	0.008	1.531	0.030	2.307	0.059	0.703832	0.000005
AZ-5	Well	NPZ	1493	252.2	Compressed liquid zone	17.968	0.374	0.007	1.816	0.036	3.030	0.077	–	–
AZ-6	Well	SPZ	2000	276.7	Compressed liquid zone	2.499	1.101	0.020	1.005	0.020	1.012	0.026	–	–
AZ-9A[b]	Well	NPZ	1810	268.3	Compressed liquid zone	17.749	0.534	0.010	1.381	0.027	1.723	0.044	0.703705	0.000005
AZ-9AD[b]	Well	NPZ	1800	267.9	Compressed liquid zone	74.968	0.333	0.006	1.550	0.031	1.971	0.050	–	–
AZ-12D	Well	SPZ	2250	286.6	Compressed liquid zone	1.088	0.621	0.011	1.352	0.027	1.708	0.044	0.703882	0.000005

Table 1 (*continued*)

Sample	Type	Field zone	Depth (m)	Bottom-hole temperature or T_G (°C)[a]	Sampled phase	± 1σ	$F(^{20}Ne)$	± 1σ	$F(^{84}Kr)$	± 1σ	$F(^{132}Xe)$	± 1σ	$^{87}Sr/^{86}Sr$	± 1σ
AZ-13	Well	NPZ	1219	235.2	Compressed liquid zone	63.137	0.432	0.008	1.719	0.034	2.610	0.067	–	–
AZ-18a	Well	SPZ	1328	242.3	Dominant liquid zone	213.095	–	–	1.864	0.037	2.317	0.059	–	–
AZ-18b	Well	SPZ	1328	242.3	Dominant liquid zone	323.282	–	–	1.625	0.051	2.414	0.085	–	–
AZ-19	Well	NPZ	1666	261.4	Compressed liquid zone	1.018	0.574	0.011	1.369	0.027	1.707	0.044	0.703789	0.000006
AZ-25	Well	SPZ	2075	279.8	Compressed liquid zone	7.076	0.382	0.007	1.758	0.035	2.831	0.072	0.703870	0.000003
AZ-26	Well	SPZ	1241	236.7	Dominant liquid zone	168.476	–	–	3.516	0.073	–	–	0.703664	0.000002
AZ-28	Well	NPZ	1680	262.1	Compressed liquid zone	5.221	0.438	0.008	1.607	0.032	2.330	0.060	0.703666	0.000004
AZ-32	Well	NPZ	1559	255.8	Compressed liquid zone	74.083	0.500	0.009	1.651	0.033	7.825	0.200	–	–
AZ-34a	Well	SPZ	1273	238.8	Dominant liquid zone	132.657	–	–	1.777	0.035	2.109	0.054	–	–
AZ-34b	Well	SPZ	1273	238.8	Dominant liquid zone	200.443	–	–	1.910	0.053	–	–	–	–
AZ-36	Well	SPZ	1050	222.6	Dominant liquid zone	38.963	0.643	0.012	1.412	0.028	1.822	0.047	–	–
AZ-38	Well	SPZ	752	194.6	Dominant steam zone	22.776	0.722	0.013	1.317	0.026	1.640	0.042	–	–
AZ-42	Well	NPZ	1814	268.5	Compressed liquid zone	0.026	0.671	0.012	–	–	1.328	0.034	0.703847	0.000004
AZ-43	Well	NPZ	1799	267.8	Compressed liquid zone	47.300	0.402	0.007	1.846	0.037	2.977	0.076	0.704102	0.000005
AZ-46	Well	SPZ	2000	276.7	Compressed liquid zone	0.237	0.816	0.015	–	–	1.240	0.032	0.703618	0.000003
AZ-47D	Well	SPZ	1520	253.7	Dominant liquid zone	15.230	0.591	0.011	1.461	0.029	1.796	0.046	0.703622	0.000003
AZ-48	Well	NPZ	2693	301.7	Compressed liquid zone	5.363	0.433	0.008	1.705	0.034	2.878	0.074	0.703960	0.000005
AZ-51a	Well	NPZ	1842	269.8	Compressed liquid zone	24.257	0.340	0.006	1.952	0.039	3.381	0.086	0.703821	0.000003
AZ-51b	Well	NPZ	1842	269.8	Compressed liquid zone	2.139	0.033	0.001	0.279	0.006	–	–	0.703821	0.000003
AZ-62a	Well	SPZ	1550	255.3	Dominant liquid zone	115.461	0.444	0.008	1.649	0.033	1.901	0.049	0.703738	0.000004
AZ-62b	Well	SPZ	1550	255.3	Dominant liquid zone	145.411	0.789	0.021	1.590	0.044	3.264	0.105	0.703738	0.000004
AZ-65	Well	NPZ	1810	268.3	Compressed liquid zone	0.064	0.514	0.009	–	–	1.658	0.042	0.703888	0.000004
AZ-66D	Well	NPZ	1773	266.6	Compressed liquid zone	0.021	–	–	–	–	0.960	0.025	0.703678	0.000004
AZ-67	Well	NPZ	1910	272.8	Compressed liquid zone	7.094	0.450	0.008	1.469	0.029	2.075	0.053	0.703739	0.000008
AZ-83a	Well	SPZ	1827	269.1	Compressed liquid zone	62.644	–	–	1.566	0.037	–	–	0.703656	0.000004
AZ-83b	Well	SPZ	1827	269.1	Compressed liquid zone	–	–	–	–	–	–	–	0.703656	0.000004
AZ-89	Well	SPZ	1876	271.3	Compressed liquid zone	6.779	–	–	1.625	0.032	2.717	0.069	0.703938	0.000004
AZ-90	Well	NPZ	2230	285.8	Compressed liquid zone	0.040	0.757	0.014	1.212	0.024	1.355	0.035	0.703820	0.000003
Maritaro 4	Spring	NPZ	–	–	–	1.511	0.488	0.009	1.592	0.032	2.674	0.068	–	–
H. Zimirao	Spring	Cuitzeo lake/ Araro	–	–	–	0.022	0.967	0.018	0.684	0.014	1.177	0.030	0.703892	0.000004
Air[c]	–	–	–	–	–	–	1.000	–	1.000	–	1.000	–	–	–—>

[a] Calculated following Garcia-Estrada et al. (2001).
[b] Sampled from different production wells.
[c] Ozima and Podosek (1983).
[d] Considering water vapor.

Table 2
He, Ne and Ar isotopic ratios as well as He/heat ratios for Los Azufres samples.

Sample	R/Ra	± 1σ	R/Rc	± 1σ	$^{20}Ne/^{22}Ne$	± 1σ	$^{21}Ne/^{22}Ne$	± 1σ	$^{38}Ar/^{36}Ar$	± 1σ	$^{40}Ar/^{36}Ar$	± 1σ	$^{3}He/Q$ (cm^3STP/J)[b]	± 1σ
AZ-2A	2.04	0.02	2.27	0.02	–	–	–	–	0.1875	0.0001	294.12	0.07	7.07E-16	1.40E-17
AZ-4	5.24	0.04	5.26	0.04	9.924	0.012	0.02798	0.00037	0.1843	0.0022	296.57	0.54	1.00E-13	1.99E-15
AZ-5	7.48	0.07	7.48	0.07	9.812	0.015	0.02907	0.00028	0.1887	0.0006	314.57	0.20	1.84E-12	3.64E-14
AZ-6	6.81	0.06	6.85	0.06	9.804	0.007	0.02889	0.00012	0.1891	0.0006	304.64	0.21	2.11E-13	4.18E-15
AZ-9A	7.93	0.09	7.93	0.09	9.806	0.023	0.02885	0.00055	0.1874	0.0006	315.13	0.40	1.80E-12	3.57E-14
AZ-9AD	7.74	0.06	7.74	0.06	9.951	0.165	0.02511	0.00484	0.1861	0.0053	364.68	1.85	7.43E-12	1.48E-13
AZ-12D	6.56	0.08	6.61	0.08	9.788	0.006	0.02900	0.00007	0.1890	0.0002	300.45	0.12	8.53E-14	1.69E-15
AZ-13	7.68	0.08	7.68	0.08	9.754	0.059	0.02963	0.00107	0.1883	0.0012	344.53	0.67	7.13E-12	1.41E-13
AZ-18a	7.66	0.08	7.66	0.08	–	–	–	–	0.1940	0.0060	597.20	3.88	2.32E-11	4.61E-13
AZ-18b	7.51	0.06	7.51	0.06	–	–	–	–	–	–	556.70	15.32	2.19E-11	6.87E-13
AZ-19	5.93	0.06	5.98	0.06	9.793	0.005	0.02877	0.00007	0.1891	0.0002	299.16	0.09	7.94E-14	1.58E-15
AZ-25	6.53	0.05	6.54	0.05	9.788	0.033	0.02986	0.00091	0.1908	0.0008	309.60	0.34	5.66E-13	1.12E-14
AZ-26	6.66	0.05	6.66	0.05	–	–	–	–	0.1991	0.0259	523.45	7.56	1.56E-11	3.25E-13
AZ-28	6.48	0.05	6.48	0.05	9.776	0.034	0.02800	0.00061	0.1901	0.0009	304.11	0.34	4.44E-13	8.80E-15
AZ-32	7.53	0.05	7.53	0.05	9.683	0.026	0.02764	0.00147	0.1891	0.0067	351.67	4.13	7.51E-12	1.49E-13
AZ-34a	7.50	0.08	7.50	0.08	–	–	–	–	0.1774	0.0043	496.10	3.11	1.44E-11	2.86E-13
AZ-34b	7.41	0.06	7.41	0.06	–	–	–	–	–	–	516.29	12.18	1.52E-11	4.26E-13
AZ-36	7.22	0.06	7.23	0.06	9.825	0.025	0.02903	0.00077	0.1857	0.0015	363.93	0.54	4.38E-12	8.70E-14
AZ-38	7.34	0.05	7.34	0.05	9.797	0.012	0.02923	0.00047	0.1888	0.0014	333.83	0.44	3.00E-12	5.96E-14
AZ-42	3.05	0.03	4.47	0.03	9.812	0.003	0.02894	0.00001	0.1876	0.0001	294.46	0.07	1.02E-15	2.02E-17
AZ-43	6.98	0.06	6.98	0.06	9.878	0.037	0.02765	0.00073	0.1889	0.0007	333.39	0.50	4.24E-12	8.41E-14
AZ-46	6.90	0.08	7.24	0.08	9.822	0.003	0.02896	0.00002	0.1879	0.0001	295.63	0.07	2.02E-14	4.02E-16
AZ-47D	7.47	0.10	7.47	0.10	9.683	0.046	0.02761	0.00091	0.1865	0.0018	325.63	0.76	1.54E-12	3.06E-14
AZ-48	6.53	0.05	6.54	0.12	9.861	0.004	0.02853	0.00032	0.1877	0.0010	301.30	0.50	3.96E-13	7.87E-15
AZ-51a	7.58	0.07	7.58	0.07	9.836	0.081	0.02741	0.00168	0.1921	0.0013	319.09	0.79	2.34E-12	4.65E-14
AZ-51b	7.37	0.04	7.37	0.04	9.812	0.020	0.02932	0.00031	0.1889	0.0009	316.02	0.60	2.01E-13	3.98E-15
AZ-62a	7.16	0.08	7.16	0.08	9.914	0.162	0.02493	0.00174	0.1869	0.0054	428.87	2.59	1.11E-11	2.21E-13
AZ-62b	7.19	0.05	7.19	0.05	9.886	0.028	0.03058	0.00190	0.2076	0.0150	410.62	9.62	1.00E-11	2.80E-13
AZ-65	5.12	0.05	5.73	0.05	9.813	0.002	0.02897	0.00002	0.1878	0.0001	295.00	0.06	4.20E-15	8.34E-17
AZ-66D	1.03	0.01	1.04	0.01	–	–	–	–	0.1878	0.0001	294.86	0.07	2.78E-16	5.52E-18
AZ-67	7.55	0.08	7.55	0.08	9.796	0.014	0.02949	0.00048	0.1891	0.0007	307.08	0.21	6.73E-13	1.34E-14
AZ-83a	6.71	0.07	6.71	0.07	–	–	–	–	0.1931	0.0204	431.80	7.87	4.51E-12	1.06E-13
AZ-83b	7.18	0.04	7.18	0.04	–	–	–	–	–	–	–	–	–	–
AZ-89	6.58	0.07	6.59	0.07	–	–	–	–	0.1923	0.0027	309.71	0.63	5.64E-13	1.12E-14
AZ-90	3.23	0.03	4.21	0.03	9.896	0.003	0.02911	0.00003	0.1876	0.0001	294.46	0.06	1.53E-15	3.04E-17
Maritaro 4	7.45	0.04	7.49	0.00	9.978	0.015	0.02935	0.00005	0.1878	0.0002	295.50	0.12	–	–
H. Zimirao	1.12	0.01	–	–	9.857	0.019	0.02905	0.00006	0.1875	0.0002	293.86	0.07	–	–
Air[a]	1.00	–	–	–	9.800	–	0.02900	–	0.1880	–	295.50	–	–	–

[a] Ozima and Podosek (1983).
[b] Calculated following Burnard et al. (1999).

1.5%, 1.3%, 1.3%, 1.5%, and 2.2%, respectively and all uncertainties are at ± 1σ level.

Water samples for strontium isotope analyses were collected directly at the water separator using a metallic container. The water was cooled to ambient temperature prior to being transferred into Nalgene® bottles. Strontium isotope analyses were conducted at Isotope Tracer Technologies Inc., Waterloo, using a Triton Thermal Ionization Mass Spectrometer with a precision ranging between 0.0002 and 0.0003% (2σ).

R/Ra values (i.e., $^3He/^4He$ ratios (R) that are normalized to the atmospheric ratio Ra, where $Ra = (1.384 \pm 0.013) \times 10^{-6}$ (Clarke et al., 1976)) were corrected with respect to an atmospheric component. This air component is potentially introduced into the system due to: a) sample contamination; b) freshwater recharge; or c) re-injection of brines at depth. R/Ra air corrected values (Rc/Ra; Table 2) were calculated as follows (Craig et al., 1978)

$$Rc/Ra = [(R/Ra)_{meas} - r]/(1 - r) \quad (1)$$

$$r = (^4He/^{20}Ne)_{ASW}/(^4He/^{20}Ne)_{meas} \quad (2)$$

where $(R/Ra)_{meas}$ is the measured R/Ra value; $(^4He/^{20}Ne)_{ASW}$ and $(^4He/^{20}Ne)_{meas}$ represent the isotopic ratios of the ASW at 12 °C (0.257; Ozima and Podosek, 1983) and that of collected samples, respectively. The temperature of 12 °C corresponds to the local mean annual air temperature (MAAT) at the LAGF (Lund and Rangel, 1995). Details on Rc/Ra uncertainty estimation are described elsewhere (Sano et al., 2006). Because Ne measurements are not available for samples AZ-2A, AZ-18, AZ-26, AZ-34, AZ-66D, AZ-83a, and AZ-89, $^4He/^{36}Ar$ ratios rather than $^4He/^{20}Ne$ values are used to derive *r* in Eq. (2) for these samples (Tables 1 and 2). For AZ-83b, R/Ra is not corrected as Ne and Ar are close to blank levels. For most samples, corrected Rc/Ra values obtained using the $^4He/^{36}Ar$ ratios are very close (within 1%) to those using $^4He/^{20}Ne$ ratios. To compare samples collected in November 2014 with those of Pinti et al. (2013), the Rc/Ra corrected based on $^4He/^{20}Ne$ ratios was adopted when available.

4. Results

Sample locations, reservoir (NPZ or SPZ), sampling date, reservoir thermodynamic conditions and Sr isotopic ratios in geothermal fluids ($^{87}Sr/^{86}Sr$) are reported in Table 1. Noble gas volume fractions (^4He, ^{20}Ne, ^{36}Ar, ^{84}Kr, and ^{132}Xe) of Los Azufres steam phase and relative abundances (F(*i*) values) are reported (Table 1). F(*i*) values are calculated by normalizing measured volume fractions to corresponding air values with ^{36}Ar as the reference isotope, i.e., $F(i) = (i/^{36}Ar)_{sample}/(i/^{36}Ar)_{air}$. F(*i*) values are fractionation factors indicating enrichment or depletion relative to the air composition and can be used as a proxy for reservoir conditions (boiling, condensate etc.) (e.g., Mazor and Bosch, 1987; Wen et al., 2016; Kennedy, 1988). Table 2 lists He, Ne and Ar isotopic ratios. Kr and Xe isotopic ratios are presented in Table 3. Atmospheric isotopic volume fractions and ratios are also provided for comparison (Tables 1, 2, and 3). Samples with noble gas isotopic

Table 3
Kr and Xe isotopic ratios for Los Azufres samples.

Sample	$^{80}Kr/^{84}Kr$	± 1σ	$^{82}Kr/^{84}Kr$	± 1σ	$^{83}Kr/^{84}Kr$	± 1σ	$^{86}Kr/^{84}Kr$	± 1σ	$^{128}Xe/^{130}Xe$	± 1σ
AZ-2A	–	–	–	–	–	–	–	–	0.4582	0.0009
AZ-4	0.03538	0.00025	0.20252	0.00047	0.20180	0.00044	0.30470	0.00067	0.5433	0.0290
AZ-5	0.04034	0.00026	0.20362	0.00138	0.20066	0.00133	0.30351	0.00216	0.4723	0.0022
AZ-6	0.04044	0.00021	0.20415	0.00101	0.20165	0.00098	0.30385	0.00163	0.4689	0.0030
AZ-9A	0.04086	0.00027	0.20517	0.00109	0.20195	0.00108	0.30181	0.00168	0.4729	0.0062
AZ-9AD	0.04098	0.00036	0.20574	0.00118	0.20188	0.00116	0.30358	0.00186	0.4841	0.0215
AZ-12D	0.03968	0.00023	0.20202	0.00117	0.20005	0.00113	0.30499	0.00187	0.4735	0.0016
AZ-13	0.04079	0.00027	0.20531	0.00123	0.20196	0.00119	0.30167	0.00192	0.4784	0.0048
AZ-18a	0.04033	0.00052	0.20516	0.00108	0.20163	0.00121	0.30128	0.00169	0.4882	0.0189
AZ-18b	–	–	0.20026	0.00319	0.19657	0.00367	0.29955	0.00462	–	–
AZ-19	0.03975	0.00026	0.20218	0.00134	0.19998	0.00130	0.30486	0.00211	0.4723	0.0013
AZ-25	0.04072	0.00023	0.20495	0.00124	0.20193	0.00115	0.30211	0.00188	0.4730	0.0025
AZ-26	0.04047	0.00104	0.20699	0.00141	0.20299	0.00199	0.30031	0.00232	–	–
AZ-28	0.04069	0.00023	0.20502	0.00119	0.20166	0.00118	0.30238	0.00181	0.4695	0.0034
AZ-32	0.03549	0.00084	0.20150	0.00105	0.20224	0.00112	0.30694	0.00129	0.4635	0.0242
AZ-34a	0.04037	0.00043	0.20571	0.00116	0.20200	0.00115	0.30143	0.00174	0.4834	0.0173
AZ-34b	0.03346	0.00204	0.20033	0.00199	0.19811	0.00212	0.30167	0.00297	–	–
AZ-36	0.04068	0.00024	0.20545	0.00116	0.20218	0.00115	0.30278	0.00185	0.4707	0.0069
AZ-38	0.04075	0.00026	0.20495	0.00119	0.20208	0.00116	0.30251	0.00186	0.4594	0.0036
AZ-42	–	–	–	–	–	–	–	–	0.4591	0.0009
AZ-43	0.04062	0.00026	0.20500	0.00124	0.20173	0.00120	0.30233	0.00194	0.4711	0.0028
AZ-46	–	–	–	–	–	–	–	–	0.4621	0.0012
AZ-47D	0.04084	0.00028	0.20524	0.00113	0.20218	0.00118	0.30141	0.00188	0.4632	0.0090
AZ-48	0.03550	0.00015	0.20296	0.00045	0.20189	0.00043	0.30555	0.00064	0.4499	0.0158
AZ-51a	0.04056	0.00028	0.20522	0.00128	0.20187	0.00126	0.30134	0.00196	0.4701	0.0046
AZ-51b	0.03565	0.00014	0.20262	0.00047	0.20181	0.00047	0.30583	0.00073	–	–
AZ-62a	0.04069	0.00056	0.20492	0.00123	0.20202	0.00135	0.30117	0.00198	0.4929	0.0186
AZ-62b	0.03556	0.00185	0.20246	0.00191	0.20424	0.00260	0.30663	0.00214	–	–
AZ-65	–	–	–	–	–	–	–	–	0.4602	0.0012
AZ-66D	–	–	–	–	–	–	–	–	0.4621	0.0009
AZ-67	0.04071	0.00026	0.20467	0.00120	0.20145	0.00118	0.30323	0.00196	0.4710	0.0026
AZ-83a	0.03904	0.00145	0.20773	0.00150	0.20232	0.00204	0.30323	0.00240	–	–
AZ-83b	–	–	–	–	–	–	–	–	–	–
AZ-89	0.04032	0.00026	0.20504	0.00122	0.20227	0.00117	0.30135	0.00183	0.4719	0.0038
AZ-90	0.03949	0.00019	0.20208	0.00097	0.20074	0.00091	0.30588	0.00155	0.4680	0.0013
Maritaro 4	0.03895	0.00011	0.20253	0.00024	0.20161	0.00028	0.30507	0.00040	0.5358	0.0178
H. Zimirao	0.06503	0.00015	0.19914	0.00029	0.19873	0.00033	0.30291	0.00049	0.4996	0.0115
Air[a]	0.03960	–	0.20217	–	0.20136	–	0.30524	–	0.4715	–

Sample	$^{129}Xe/^{130}Xe$	± 1σ	$^{131}Xe/^{130}Xe$	± 1σ	$^{132}Xe/^{130}Xe$	± 1σ	$^{134}Xe/^{130}Xe$	± 1σ	$^{136}Xe/^{130}Xe$	± 1σ
AZ-2A	6.6000	0.0118	5.2550	0.0086	6.7260	0.0131	2.6064	0.0054	2.2206	0.0038
AZ-4	6.5331	0.0417	5.2029	0.0315	6.6335	0.0422	2.5690	0.0166	2.1791	0.0154
AZ-5	6.4646	0.0152	5.1910	0.0124	6.5964	0.0190	2.5598	0.0080	2.1769	0.0056
AZ-6	6.5256	0.0212	5.2026	0.0171	6.6421	0.0257	2.5770	0.0112	2.1949	0.0082
AZ-9A	6.4781	0.0479	5.1952	0.0387	6.5799	0.0501	2.5530	0.0197	2.1693	0.0168
AZ-9AD	6.4872	0.1241	5.1404	0.0991	6.6063	0.1278	2.6013	0.0525	2.2147	0.0458
AZ-12D	6.4706	0.0114	5.1925	0.0094	6.5968	0.0163	2.5585	0.0070	2.1767	0.0044
AZ-13	6.4351	0.0364	5.1702	0.0296	6.5278	0.0396	2.5347	0.0164	2.1542	0.0132

Table 3 (*continued*)

Sample	$^{129}Xe/^{130}Xe$	± 1σ	$^{131}Xe/^{130}Xe$	± 1σ	$^{132}Xe/^{130}Xe$	± 1σ	$^{134}Xe/^{130}Xe$	± 1σ	$^{136}Xe/^{130}Xe$	± 1σ
AZ-18a	6.4706	0.1225	5.1375	0.0984	6.5117	0.1246	2.5422	0.0529	2.1189	0.0429
AZ-18b	6.3666	0.4746	–	–	6.1801	0.4583	–	–	–	–
AZ-19	6.4773	0.0113	5.1957	0.0095	6.6042	0.0160	2.5636	0.0069	2.1799	0.0045
AZ-25	6.5189	0.0199	5.2138	0.0167	6.6464	0.0238	2.5811	0.0099	2.1964	0.0074
AZ-26	–	–	–	–	–	–	–	–	–	–
AZ-28	6.4963	0.0234	5.1941	0.0193	6.6290	0.0279	2.5707	0.0116	2.1848	0.0087
AZ-32	6.5004	0.0673	5.2338	0.0542	6.6564	0.0700	2.5781	0.0286	2.1895	0.0257
AZ-34a	6.5204	0.1144	5.1861	0.0927	6.5779	0.1169	2.5635	0.0466	2.1380	0.0406
AZ-34b	–	–	–	–	–	–	–	–	–	–
AZ-36	6.4817	0.0403	5.1460	0.0326	6.6039	0.0428	2.5679	0.0178	2.1827	0.0151
AZ-38	6.5686	0.0243	5.2403	0.0197	6.6895	0.0281	2.5912	0.0120	2.2172	0.0092
AZ-42	6.6348	0.0137	5.2799	0.0096	6.7649	0.0137	2.6160	0.0056	2.2396	0.0038
AZ-43	6.4605	0.0171	5.1787	0.0142	6.5876	0.0220	2.5567	0.0091	2.1696	0.0064
AZ-46	6.6081	0.0139	5.2798	0.0108	6.7262	0.0151	2.6010	0.0061	2.2252	0.0043
AZ-47D	6.4560	0.0649	5.1775	0.0522	6.5263	0.0666	2.5243	0.0265	2.1436	0.0234
AZ-48	6.5180	0.0296	5.2150	0.0231	6.6267	0.0316	2.5662	0.0124	2.1800	0.0104
AZ-51a	6.4403	0.0272	5.1662	0.0222	6.5718	0.0301	2.5415	0.0124	2.1631	0.0101
AZ-51b	–	–	–	–	–	–	–	–	–	–
AZ-62a	6.5501	0.1101	5.1998	0.0905	6.5983	0.1127	2.5525	0.0468	2.1675	0.0393
AZ-62b	6.5244	0.1997	5.1950	0.1617	6.5626	0.1993	2.5432	0.0866	2.2376	0.0759
AZ-65	6.5876	0.0124	5.2849	0.0101	6.7260	0.0148	2.6091	0.0060	2.2302	0.0043
AZ-66D	6.5803	0.0093	5.2615	0.0074	6.7134	0.0113	2.6007	0.0049	2.2251	0.0031
AZ-67	6.4890	0.0217	5.1946	0.0178	6.6031	0.0259	2.5614	0.0109	2.1782	0.0080
AZ-83a	–	–	–	–	–	–	–	–	–	–
AZ-83b	–	–	–	–	–	–	–	–	–	–
AZ-89	6.6156	0.0230	5.3004	0.0190	6.7645	0.0273	2.6316	0.0116	2.2537	0.0090
AZ-90	6.5375	0.0118	5.2029	0.0097	6.6555	0.0173	2.5784	0.0073	2.1925	0.0047
Maritaro 4	6.5234	0.0236	5.2347	0.0188	6.6217	0.0254	2.5679	0.0099	2.1733	0.0086
H. Zimirao	6.4686	0.0141	5.1875	0.0110	6.5681	0.0141	2.5540	0.0058	2.1636	0.0049
Air[a]	6.4960	–	5.2130	–	6.6070	–	2.5630	–	2.1760	—>

[a] Ozima and Podosek (1983).

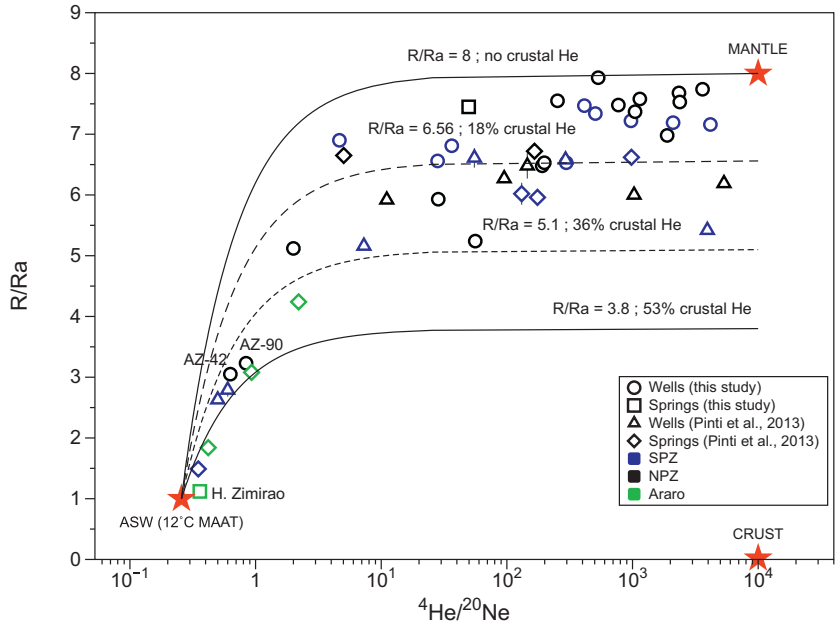

Fig. 2. R/Ra ratio as a function of $^{4}He/^{20}Ne$ ratio for collected fluid samples in this study as well as samples from (Pinti et al., 2013). All data can be interpreted as a mixing of an ASW component (R/Ra = 1, $^{4}He/^{20}Ne$ = 0.257; Ozima and Podosek, 1983) and a terrigenic component including crustal (R/Ra = 0.02, $^{4}He/^{20}Ne$ = 10,000) and mantle (R/Ra = 8, $^{4}He/^{20}Ne$ = 10,000) noble gases (Graham, 2002; Morikawa et al., 2008; Oxburgh et al., 1986). (For interpretation of the references to colour in this figure legend, the reader is referred to the web version of this article.)

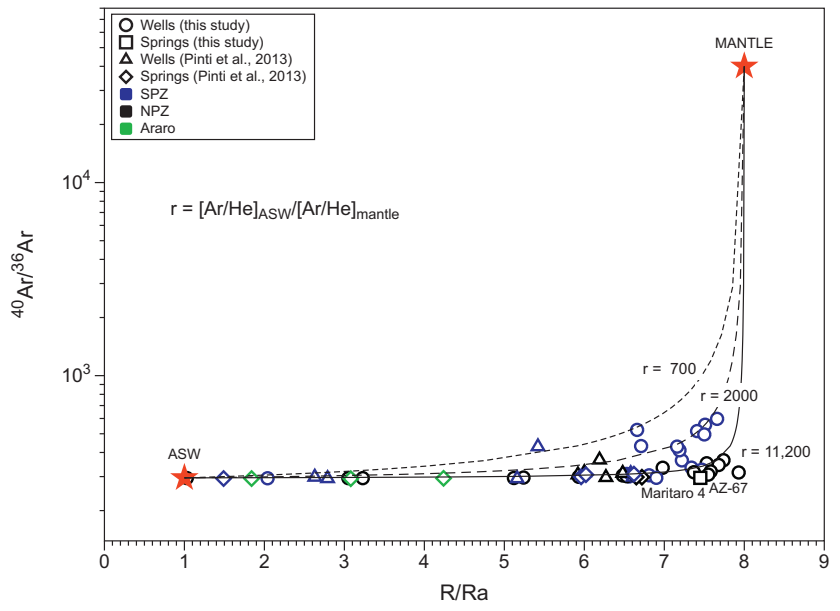

Fig. 3. $^{40}Ar/^{36}Ar$ versus R/Ra for samples in this study and in Pinti et al. (2013). Corresponding values in the air and mantle are also shown for comparison (Burnard et al., 1997; Ozima and Podosek, 1983). The curves, representing the mixing between mantle- and air-derived helium and argon, are plotted for different curvature parameters *r*. See text for details. (For interpretation of the references to colour in this figure legend, the reader is referred to the web version of this article.)

volume fractions close to blank levels are not reported as these have poor isotopic measurement precision.

R/Ra values range from 1.03 ± 0.01 to 7.93 ± 0.09. Most samples (32 out of 37) yield R/Ra ratios > 5 which indicates the presence of a highly dominant mantle origin for helium. The highest R/Ra value of 7.93 ± 0.09, measured in well AZ-9A is very close to that of a pure upper mantle component representative of Mid Ocean Ridge Basalts (MORB; R/Ra = 8 ± 1; Graham, 2002). Interestingly, the highest reservoir temperature of 347 °C was measured in this same well (Molina Martínez, 2013).

Rc/Ra ratios for all samples range from 1.04 ± 0.01 to 7.93 ± 0.09 pointing to mixing between two distinct helium reservoirs, the crust and the upper mantle. Rc/Ra and R/Ra values are not significantly different for most samples (Table 2), suggesting minor helium atmospheric contributions.

$^{20}Ne/^{22}Ne$ and $^{21}Ne/^{22}Ne$ values vary from 9.68 ± 0.03 to 9.98 ± 0.02 and from 0.0249 ± 0.0017 to 0.0306 ± 0.0019, respectively. Some of these values are greater than corresponding air values ($^{20}Ne/^{22}Ne$ = 9.80 and $^{21}Ne/^{22}Ne$ = 0.0290; Ozima and Podosek, 1983) and suggest the presence of crustal (Kennedy et al., 1991) and mantle (Sarda et al., 1988) Ne. $^{40}Ar/^{36}Ar$ isotopic ratios range from 293.9 ± 0.1 to 597.2 ± 3.9 with most samples (26 out of 37) presenting values greater than that of air (i.e., 295.5; Ozima and Podosek, 1983). These elevated $^{40}Ar/^{36}Ar$ values point to the presence of crustal and/or mantle ^{40}Ar in most samples.

5. Discussion

5.1. Mixing of atmosphere-, crust-, and mantle-derived helium and argon

5.1.1. Atmospheric He and Ar

Fig. 2 plots R/Ra values as a function of $^{4}He/^{20}Ne$ ratios for all fluid samples collected in this study as well as for earlier LAGF fluid data (Pinti et al., 2013). R/Ra values are distinct for the air, crust and mantle

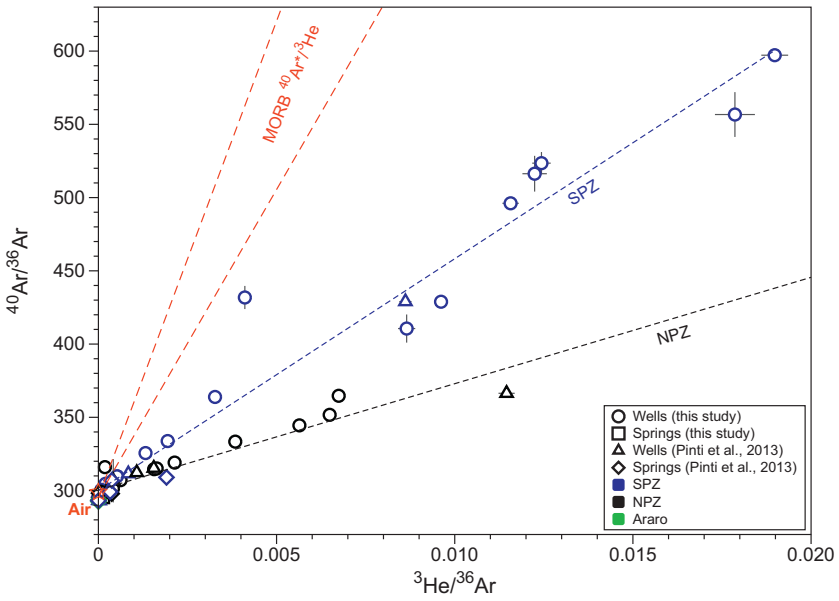

Fig. 4. $^{40}Ar/^{36}Ar$ versus $^3He/^{36}Ar$ ratios for fluid samples from both this study and previous study (Pinti et al., 2013). Corresponding linear regression lines are shown for samples in NPZ and SPZ, respectively with slope be equal to the $^{40}Ar^*/^3He$ ratio. Regression lines for MORB are plotted following $^{40}Ar^*/^3He$ ratios from Burnard et al. (1997) and Staudacher et al. (1989). Noble gas isotopic ratios in air are also shown for comparison (hollow star). (For interpretation of the references to colour in this figure legend, the reader is referred to the web version of this article.)

end-members. Assuming R/Ra values in the mantle (MORB) and in the crust to be 8 and 0.02 (Graham, 2002; Oxburgh et al., 1986), respectively, leads to mantle He contributions varying between 12.8% and 99.1% in all samples. As observed for R/Ra, the terrigenic (i.e., crust and/or mantle) $^4He/^{20}Ne$ value is also significantly higher (~10,000, Morikawa et al., 2008) than the air value (0.318, Ozima and Podosek, 1983), rendering this elemental ratio a useful discriminant for atmospheric and terrigenic noble gas source contributions. Except for production wells AZ-42, AZ-90 and the *Hervideros de Zimirao* hot spring, the contribution of mantle and crustal helium is dominant for most samples collected. R/Ra values for wells AZ-42 and AZ-90 are 3.05 ± 0.03 and 3.23 ± 0.03, respectively (Table 2) while their corresponding Rc/Ra values are 4.47 ± 0.03 and 4.21 ± 0.03, respectively (Table 2). This points to a maximum crustal He contribution of 44–48%. The helium signal from the *Hervideros de Zimirao* hot spring in the *Araró* area of the Cuitzeo Lake (Fig. 1B) is likely derived from air contamination as indicated by the $^4He/^{20}Ne$ ratio of 0.361, close to that of the atmosphere (0.318; Ozima and Podosek, 1983) and clearly distinct from that of ASW at 12 °C (0.257; Table 1; Fig. 2). This spring is an intermittent geyser rendering sampling challenging. It is located very close to the sample *Araró north* of Pinti et al. (2013), which yielded Rc/Ra of 4.17 ± 0.05, the typical He isotopic signature for the *Araró* locality (Pinti et al., 2013). Because air contamination is likely, this sample will not be discussed further. The low R/Ra value (2.04 ± 0.02) of well AZ-2A points to the presence of a significant air component resulting from re-injection (Pinti et al., 2013). The lowest R/Ra value of 1.03 ± 0.01 observed at well AZ-66D, suggests either the presence of a significant re-injection component or air contamination.

The atmosphere contains 1% of argon by volume and very little ^3He. In contrast, argon in the mantle is present at low levels while the ^3He content is high. This leads to rapid dilution of mantle argon but not of mantle helium when air is added to a magmatic fluid (Pinti et al., 2017). R/Ra remains mostly unaffected by the addition of freshwater until its proportion in the mixture reaches at least 80% of the total amount of fluid (Pinti et al., 2017). Thus, identification of mantle Ar is nearly impossible based solely on the $^{40}Ar/^{36}Ar$ ratios. Fig. 3 presents $^{40}Ar/^{36}Ar$ ratios as a function of R/Ra for LAGF fluid samples. The dilution effect is apparent in some samples (e.g., AZ-67 and hot spring

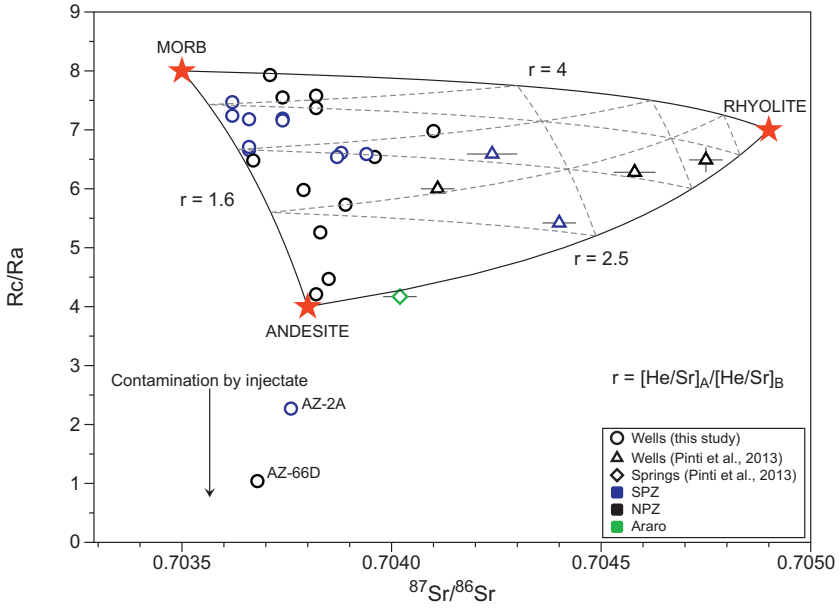

Fig. 5. Rc/Ra value versus $^{87}Sr/^{86}Sr$ ratio measured in samples from this study and Pinti et al. (2013). Measured data points to mixing of three magmatic sources for He and Sr isotopes: (1) a pure mantle He (Rc/Ra = 8) and Sr (0.7035; Donnelly et al., 2004) source; (2) a mantle helium (Rc/Ra = 7) with some radiogenic Sr (0.7049; Verma et al., 2005) possibly resulting from the late rhyolitic volcanism; and (3) a fossil mantle He component (Rc/Ra = 4.0) with some radiogenic Sr (0.7038; Verma et al., 2005), corresponding possibly to the Miocene andesite reservoir. Mixing ternary hyperbola diagram between the three end-members have been calculated using the software Isonc 1.0 (Phillips and Koch, 2002). (For interpretation of the references to colour in this figure legend, the reader is referred to the web version of this article.)

Maritaro 4) which display high R/Ra values while yielding $^{40}Ar/^{36}Ar$ ratios close to that of the atmosphere and thus, that of ASW (Table 2).

5.1.2. Crustal- and mantel-derived He and Ar

Regression analysis indicates that the contribution of crustal helium is up to 53% and 18% for fluid samples in the NPZ and SPZ, respectively (dashed lines in Fig. 2), suggesting that NPZ fluids have longer residence times, allowing crustally produced ^4He to further accumulate.

Comparison of fluid samples between this study and that of Pinti et al. (2013) suggests that the overall contribution of atmospheric helium remained unchanged for both, the NPZ and SPZ between 2007/2009 (Fig. 2; Pinti et al., 2013) and 2014. It is also worth noting that, with a few exceptions, fluid samples in this study with higher R/Ra values tend also to have higher $^{40}Ar/^{36}Ar$ ratios, above the air value of 295.5 (Table 2; Fig. 3), suggesting the presence of terrigenic argon in some samples, of either mantle or crustal origin.

The $^{40}Ar/^{36}Ar$ and R/Ra ratio end-members in the mantle are assumed to be 40,000 (Burnard et al., 1997) and 8 ± 1 (Graham, 2002), respectively, while the atmospheric $^{40}Ar/^{36}Ar$ and R/Ra ratios are 295.5 and 1 (Ozima and Podosek, 1983), respectively. The theoretical mixing line (solid curve in Fig. 3) between a pure mantle and an ASW end-member should be a hyperbola with the curvature parameter $r = [Ar/He]_{ASW}/[Ar/He]_{mantle}$ equal to 11,200. This value is obtained from a mantle Ar/He ratio of 0.704 (calculated from data of Moreira et al. (1998)) and a Ar/He ratio of ASW at 12 °C of 7982 (calculated from solubility data of Smith and Kennedy (1983)). Many samples fall on this curve (i.e., $r = 11{,}200$) while several samples do not plot on this mixing hyperbola. Best fitting suggests mixing hyperbolas with decreasing curvature parameter r ranging from 2000 to 700. Because the ASW Ar/He end-member displays little variation under the recharge conditions in the LAGF (Ar/He ratio in ASW varies within a factor of 2 for the range of recharge temperatures of 4–31 °C; Lund and Rangel, 1995), it requires ca. a 5–15 times higher Ar/He ratio of the magmatic source to explain these outliers (Fig. 3).

Solubility-controlled fractional (Rayleigh) degassing of the melt could be assumed as the main process of mantle volatile addition to geothermal fluids (e.g., Paonita et al., 2012; Burnard et al., 2004). Because Ar is much less soluble than He in the melt, degassed volatiles will have a Ar/He ratio much higher than that in the residual melt (Burnard et al., 2004), resulting in a much lower curvature parameter r, as observed in Fig. 3.

An alternative hypothesis is the addition of crustal Ar (Pinti et al., 2017). To test this hypothesis, $^{40}Ar/^{36}Ar$ ratios are plotted versus $^3He/^{36}Ar$ ratios (Fig. 4). Fig. 4 shows that NPZ and SPZ fluid samples lie on two distinct regression lines representing mixing between a freshwater/atmospheric component (low $^{40}Ar/^{36}Ar$ and $^3He/^{36}Ar$ values), and the subsurface fluid enriched in terrigenic He and Ar, as shown by higher $^{40}Ar/^{36}Ar$ and $^3He/^{36}Ar$ ratio values. The relation between $^{40}Ar/^{36}Ar$ ratios and $^3He/^{36}Ar$ ratios have been often observed in fluid inclusions associated with hydrothermal-magmatic ore deposits (e.g., Burnard et al., 1999; Burnard and Polya, 2004) and interpreted as a mixing between a modified ASW fluid and a hydrothermal component enriched in both $^{40}Ar^*$ (i.e., crustal ^{40}Ar) and ^3He.

The slope of the regression line reflects the average $^{40}Ar^*/^3He$ ratio of the associated fluid sample (Burnard and Polya, 2004). Estimated $^{40}Ar^*/^3He$ values are 16,220 and 8060 for SPZ and NPZ, respectively, with a corresponding correlation coefficient r^2 equal to 0.96 and 0.85, respectively. These estimated values are much lower than the $^{40}Ar^*/^3He$ values expected for the mantle, i.e., 42,000–60,000 (Burnard et al., 1999; Staudacher et al., 1989) and even lower than the estimated value for the bulk continental crust of 2×10^7 (Stuart et al., 1995). He in LAGF fluids is enriched by a factor of 3–7 relative to Ar, with respect to the mantle composition (Fig. 4). The lower $^{40}Ar^*/^3He$ ratio in the LAGF hydrothermal fluid compared to a pure mantle source calls for a local source of terrigenic Ar which is much less mobile than He in rocks. The terrigenic Ar could be produced in local volcanites such as the rhyolites that have a K content up to 6 wt% (Pradal and Robin, 1994) and subsequently released into the fluid with mantle He. Emplacement of the magma body that provided heat to the field could have enhanced degassing of rocks in this area. This might facilitate the release of crustally-produced Ar from the rock that eventually over-imprinted the possible original mantle Ar signatures in the magma body. It is unclear why we have a net dichotomy with wells from the NPZ showing lower $^{40}Ar^*/^3He$ than those from the SPZ (Fig. 4). This could be due to either 1) a lithological control in the release of He and Ar, within the southern part of the LAGF where most of the rhyolite intrusions outcrops (Pradal and Robin, 1994), or; 2) boiling in the reservoir (Burnard and Polya, 2004). Because He is less soluble in water than Ar, the original $^{40}Ar^*/^3He$ fluid ratio could be strongly fractionated during boiling in the reservoir, with He enriched compared to Ar in the sampled fluid (e.g., Pinti et al., 2013; Mazor and Truesdell, 1984). Interestingly, the NPZ reservoir seems to be more affected by boiling than that in the SPZ (Arellano et al., 2015).

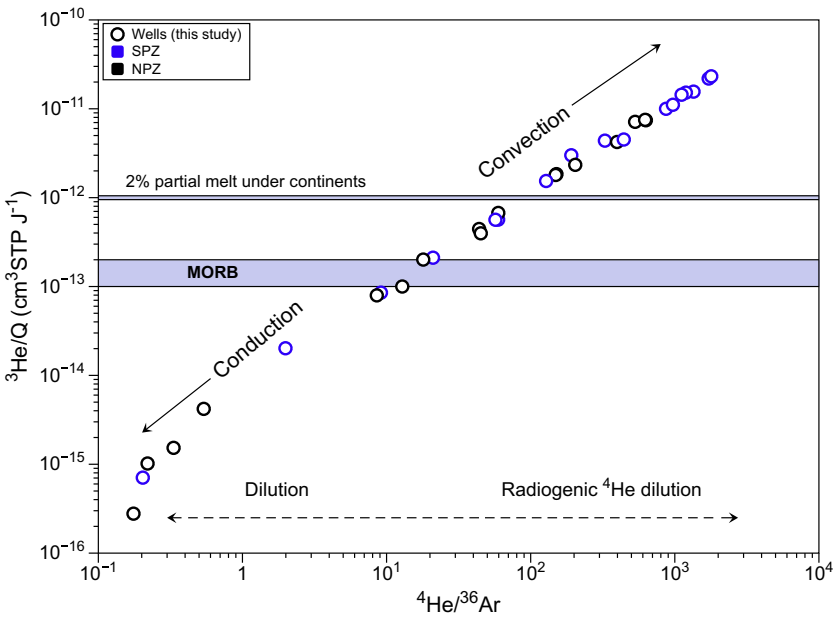

Fig. 6. $^3He/Q$ vs. $^4He/^{36}Ar$ for fluid samples in both NPZ (black open circles) and SPZ (blue open circles). The $^3He/Q$ value in MORB is shown for comparison (Burnard and Polya, 2004). Corresponding $^3He/Q$ value in mantle magma below the continents is estimated as 1×10^{-12} cm^3 STP J^{-1} by assuming 2% partial melts during melt generation (Burnard and Polya, 2004). (For interpretation of the references to colour in this figure legend, the reader is referred to the web version of this article.)

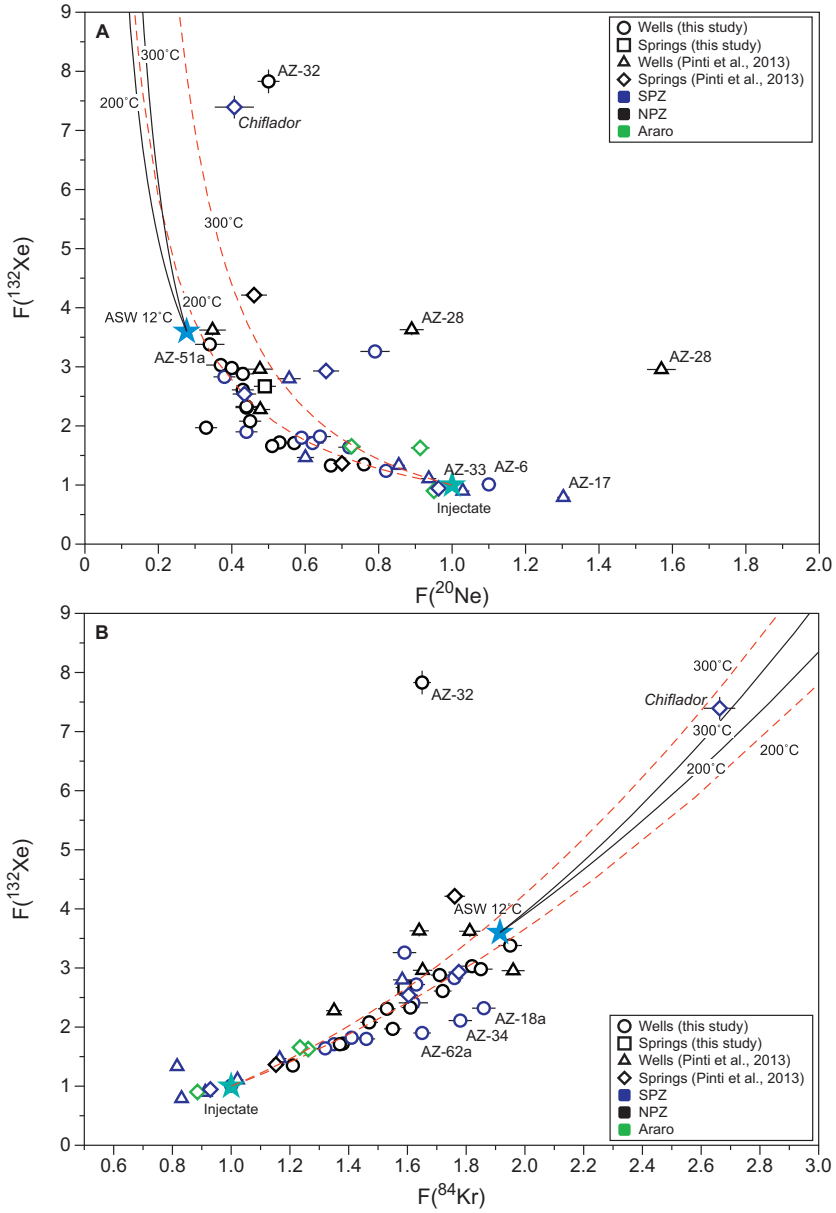

Fig. 7. (A) F(^{132}Xe) vs. F(^{20}Ne) and (B) F(^{132}Xe) vs. F(^{84}Kr) values for fluid samples in this study and Pinti et al. (2013). Corresponding values in ASW at 12 °C and injectate (air-like) are shown for comparison (Crovetto et al., 1982; Ozima and Podosek, 1983). Calculated F values in residual liquid following Rayleigh fractionation from initial injectate (red dashed curves) or initial ASW at 12 °C (black solid curves) for boiling temperatures of 200 and 300 °C have been reported. (For interpretation of the references to colour in this figure legend, the reader is referred to the web version of this article.)

5.2. Heat: Sources, timing and transport

One of the unresolved questions of the Los Azufres hydrothermal system relates to the origin of its heat source. Miocene-Pliocene andesites are too old to supply high enthalpy to the field. Conductive models in Los Azufres (Garcia-Estrada et al., 2001) suggested that the intrusion should be no older than 0.4 Ma to maintain the current high enthalpy in the field. This limits the choice to Quaternary rhyolitic and dacitic magmas that erupted between 0.15 Ma and 30 kyrs (Pradal and Robin, 1994). Based on sparse Sr isotopic data, Pinti et al. (2013) preliminarily concluded that the potential sources of mantle He and heat could be mafic magmas at depth.

Fig. 5 suggests mixing of three end-members for most samples (this study and Pinti et al., 2013). The first end-member (labeled *MORB*; Fig. 5) is a MORB-like mantle source with Rc/Ra of 8 and ^{87}Sr/^{86}Sr ratio of 0.7035. This latter value is slightly more radiogenic than the typical N-MORB, resembling more closely that of *E*-MORB (Donnelly et al., 2004). This MORB-like parental magma might be the one giving rise to the *La Calabaza* and *Llano Grande* mafic lava flow sequences at around 0.6 Ma (Pradal and Robin, 1994). The second end-member (labeled *Andesite*; Fig. 5) has a lower Rc/Ra value of ca. 4.0 (Pinti et al., 2013) and a ^{87}Sr/^{86}Sr ratio of 0.7038, similar to that of Miocene andesites (Verma et al., 2005). The lower Rc/Ra value might be caused by "magma aging", i.e., internal production of radiogenic ^{4}He from U and Th that lower the original Rc/Ra ratio of the magmatic source (Kennedy and van Soest, 2006). The third end-member (labeled *Rhyolite*; Fig. 5) has a ^{87}Sr/^{86}Sr ratio of 0.7049 (typical of local dacites and rhyolites; Verma et al., 2005) and Rc/Ra of ca. 7 that is slightly lower than that of mafic end-member but higher than that of typical intermediate to felsic rocks (Hilton et al., 1993a, 1993b). Although felsic rocks contain greater amounts of U and Th than mafic ones, the younger ages of the felsic units could explain why "magma aging" has not significantly modified the initial Rc/Ra of the rhyolitic magma in a similar manner to that observed for Miocene andesites. This dacite-rhyolite end-member

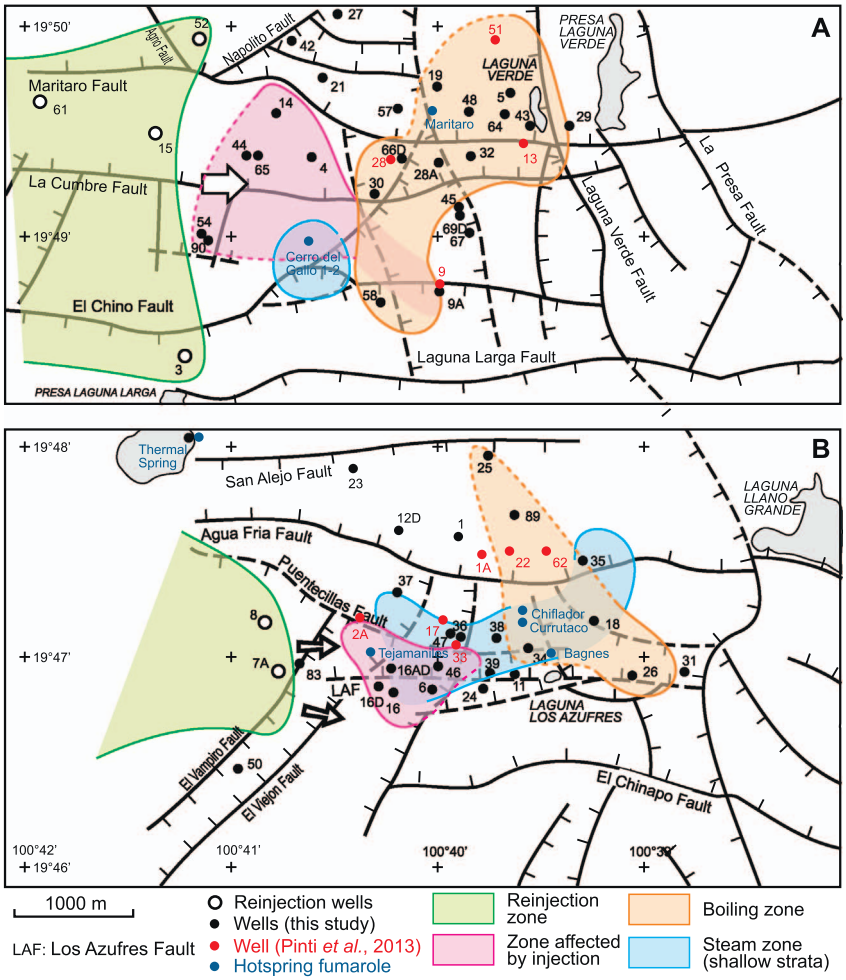

Fig. 8. LAGF map (redrawn from Fig. 1C) with main tectonic features. The area of re-injection of used brines (injectate), production area affected by re-injection, the boiling zone, and the steam-dominated zone are modified from Barragán et al. (2005) and Pinti et al. (2013). Dashed contours indicate the extension of the boiling zone and area affected by the injectate as inferred from fractionation patterns of noble gases measured in this study. (For interpretation of the references to colour in this figure legend, the reader is referred to the web version of this article.)

and the MORB-like basalts end-member are likely the source of heat and mantle volatiles in LAGF.

A first order estimation of the timing of the parental magmas' emplacement using a simple magma aging model was carried out. Assuming an initial MORB-like mantle Rc/Ra of 8, a ^{4}He content in melts of 10^{-7} to 10^{-9} cm^{3}STP/g (e.g., Kennedy and van Soest, 2006), and U and Th content in MORB-like basalts of 0.23 and 0.75 ppm, respectively (Kelemen et al., 2004; Salters and Stracke, 2004), shows that 500 to < 50,000 years would be required to bring an original Rc/Ra value of 8 to 7.8, a value very close to the maximum value measured in the LAGF fluids (Table 2). Assuming the same initial Rc/Ra value and a similar ^{4}He content in melts but U and Th contents in felsic rocks of 2.5 and 10.2 ppm (Condie, 1993), shows that between 250 and 25,000 years would be required to lower the initial Rc/Ra ratio to 7 (rhyolite end-member; Fig. 5). These estimated time lengths for a single magma body cooling is comparable to results from cooling models of small size plutons (a few kilometers diameter) (e.g., Elders et al., 1984; Hayba and Ingebritsen, 1997). These calculations suggest that the LAGF heat sources were active from the Late Pleistocene to Holocene, and possibly, in more recent times, supplying high enthalpy currently observed in the LAGF.

In addition to mantle He and Ar, magma will transport heat (Q) to the LAGF hydrothermal system. ^{3}He/Q values in hydrothermal fluids might be fractionated due to magmatic processes (e.g., Castro et al., 2005). In particular, heat transport by conduction could transfer heat but not helium into the hydrothermal system while convection will transport helium more rapidly than heat. Thus, the study on ^{3}He/Q values will help discriminate between heat transfer mechanisms, i.e., convection vs. conduction. ^{3}He/Q values of fluid samples in this study were calculated as follows (Burnard et al., 1999; Burnard and Polya, 2004; Turner and Stuart, 1992):

$$^3\mathrm{He/Q} = {}^3\mathrm{He}/^{36}\mathrm{Ar} \times {}^{36}\mathrm{Ar}_{\mathrm{ASW}}/(Cp \times \theta) \quad (3)$$

where Cp and θ are specific heat capacity (4.4 J K^{-1} g^{-1}; Burnard et al., 1999) and temperature excess (°C) with respect the local MAAT of 12 °C (Table 1). ^{3}He/^{36}Ar ratios are measured values while ^{36}Ar$_{ASW}$ represents ^{36}Ar concentration in ASW at 12 °C (1.241×10^{-6} cm^3 STP cm^{-3}). Calculated ^{3}He/Q ratios should be minimum estimates as air contamination tends to lower the ^{3}He/^{36}Ar ratios (Burnard and Polya, 2004). Bottom hole temperature (T_G) at each production well was estimated from the average geothermal gradient extrapolated to all the LAGF by Garcia-Estrada et al. (2001) and based on initial direct temperature measurements in the drilled wells (Table 1).

Estimated ^{3}He/Q ratios of LAGF fluids range from 2.78×10^{-16} cm^3 STP J^{-1} to 2.32×10^{-11} cm^3 STP J^{-1}. Most wells (25 out of 35) display ^{3}He/Q values (Table 2) much higher than that in the MORB ($0.1–0.2 \times 10^{-12}$ cm^3 STP J^{-1}; Baker and Lupton, 1990; Lupton et al., 1995). Assuming a 2% partial melt during melt generation underneath the continents (Martel et al., 1989), associated ^{3}He/Q ratio in the magma is estimated to be $\leq 1 \times 10^{-12}$ cm^3 STP J^{-1}

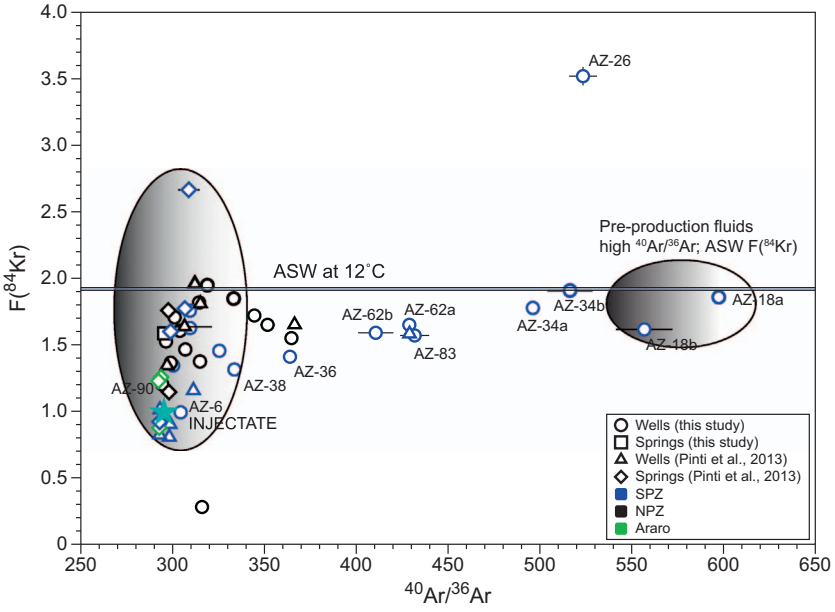

Fig. 9. F(^{84}Kr) vs. ^{40}Ar/^{36}Ar ratios for fluid samples in this study and previous study (Pinti et al., 2013). Corresponding values of injectate with air composition, ASW at 12 °C, and pre-production fluid are shown for comparison (Ozima and Podosek, 1983). (For interpretation of the references to colour in this figure legend, the reader is referred to the web version of this article.)

(Burnard and Polya, 2004), which is still lower than those of many samples (18 out of 35; Fig. 6). High ^{3}He/Q values in many of LAGF samples suggest heat transport by convection although a conductive mechanism is also indicated by low ^{3}He/Q ratios of some samples (Fig. 6). Among those fluid samples with high ^{3}He/Q values, there are 11 and 14 samples collected from NPZ and SPZ, respectively. Therefore, the heat transfer mechanism in NPZ and SPZ seems to be similar and cannot account for chemical or isotopic differences observed in these two production zones.

5.3. Re-injection, boiling, and steam separation effects in LAGF

Re-injection of used brines (injectate) in LAGF started in 1982, rapidly causing boiling and phase separation (Pinti et al., 2013). Here, injectate refers to a mixture of steam, water, and air (Pinti et al., 2017). The noble gas concentration in injectate is normally 100 to 1000 times lower than that in ASW (Kennedy et al., 2000) while isotopic ratios are atmospheric (Pinti et al., 2017). Reinjection and boiling can be identified by plotting F(^{132}Xe) vs. F(^{20}Ne) and F(^{132}Xe) vs. F(^{84}Kr) (Fig. 7A and B). Because light noble gases will have lower solubility in water (Smith and Kennedy, 1983), boiling will lead to a decrease of F(^{20}Ne) and an increase of F(^{132}Xe) and F(^{84}Kr) in the residual liquid phase. Predicted F(i) values in the residual liquid can be estimated by assuming a Rayleigh fractionation (Pinti et al., 2013) process:

$$\left(\frac{i}{^{36}Ar}\right)_{residual} = \left(\frac{i}{^{36}Ar}\right)_{0} \times \frac{1 - f^{\frac{K_w^i}{K_w^{Ar}}}}{1 - f} \quad (4)$$

where f is the fraction of ^{36}Ar remaining in the residual water. The $\left(\frac{i}{^{36}Ar}\right)_0$ represents the elemental abundance ratio in the initial water, in which i represents ^{20}Ne, ^{84}Kr or ^{132}Xe. $K_w{}^i$ and $K_w{}^{Ar}$are the Henry's constants of gas i and Ar in water, which are calculated using data from Crovetto et al. (1982) and Smith (1985). Pre-production fluids are expected to have elemental abundance ratios $\left(\frac{i}{^{36}Ar}\right)_0$ equal to that of ASW (here calculated at MAAT of 12 °C; Fig. 7A and B).

At first glance, the F(^{20}Ne), F(^{84}Kr), and F(^{132}Xe) values of most LAGF fluids plot between predicted ratios for the ASW at 12 °C and the injectate, suggesting a possible mixing. This would indicate that the injectate has extended throughout the entire field and impacted different areas to varying extents, from west to east. Except for the *Chiflador* fumarole sampled by Pinti et al. (2013), no fluids plot along the black solid curves departing from the ASW composition. These curves represent the expected evolution of the F(i) values during boiling (as calculated from Eq. (4)), at reservoir temperatures of 200 and 300 °C (i.e., the minimum and maximum values calculated in the reservoir; Table 1; Segovia et al., 2005; Barragán et al., 2005).

This result is surprising because numerous studies have clearly demonstrated that boiling is affecting the LAGF reservoir (e.g., Barragán et al., 2005). This apparent contradiction can be resolved if we assume that pre-production fluids mixed with the injectate (shifting F(i) values towards the unity), and then fluids were affected by boiling. This evolution is represented in Fig. 7A and B by the red dashed lines departing from the injectate composition. Alternatively, observed F(i) values could be explained by the mixing of injectate and the condensate (steam phase) derived from ASW boiling at reservoir temperatures. In either scenario, the impact of injectate should be significant and the boiling process should be taken into account.

Some samples, e.g., AZ-6 (this study) and AZ-17 and AZ-33 (Pinti et al., 2013), deviate from the general trend (Fig. 7). These samples are compatible with a sampled steam phase. In addition, calculated F(i) values in AZ-28 samples are distinct due to different efficiencies in the steam/liquid separator at the well head (Pinti et al., 2013).

Samples AZ-6, AZ-38, AZ-46, and AZ-90 have the highest F(^{20}Ne) values (> 0.7), similar to that of injectate (Fig. 7A and B) as well as lowest F(^{84}Kr) and/or F(^{132}Xe) values, suggesting that these samples have been significantly impacted by the injectate. In addition, well AZ-2A with a F(^{132}Xe) value of 0.928, reflects the presence of significant air contamination, as suggested by Pinti et al. (2013). Samples AZ-2A, AZ-6, AZ-46, and AZ-90 that show injectate-like F(i) values are located close to the western re-injection zone (Fig. 1C). This is also an indication that the reinjection zone has further spread since the last sampling campaign in 2007/2009 (Fig. 8).

Solubility-controlled boiling and condensation processes have fractionated noble gas abundances in many wells (Fig. 7A and B). For example, fluid samples AZ-5, AZ-43, and AZ-62 display fractionated F(i) confirming that these wells are located within the boiling zone as previously suggested by Barragán et al. (2005) and Pinti et al. (2013). However, production wells AZ-19 in NPZ, and AZ-25 and AZ-34 in the SPZ, which were not sampled for noble gas analyses by Pinti et al. (2013), also show highly fractionated F(i) values pointing to the occurrence of boiling processes (Table 1). These three wells are out of the previously estimated boiling zone, and suggest that the boiling zone has further extended to the north and west since the last sampling campaign

in 2007/2009 (Fig. 8).

Mixing of pre-production reservoir fluid and injectate is also indicated in Fig. 9 which plots F(^{84}Kr) ratio as a function of ^{40}Ar/^{36}Ar values of fluid samples from both this study and Pinti et al. (2013). Production wells in Fig. 9 might be divided into two groups. The first group (e.g., AZ-18, AZ-34, AZ-36, AZ-62 and AZ-83) shows a correlation between F(^{84}Kr) and ^{40}Ar/^{36}Ar values (r^2 = 0.71) which appears to point to mixing between one end-member with high ^{40}Ar/^{36}Ar values (> 500) and unfractionated F(^{84}Kr) which corresponds likely to the pre-production fluid, and the other end-member characterized by atmospheric F(^{84}Kr) and ^{40}Ar/^{36}Ar ratios which might be the injectate (Pinti et al., 2017). The second group is scattered with respect to F (^{84}Kr) ratios while displaying ^{40}Ar/^{36}Ar values close to the atmospheric value of 295.5. This group might represent fluids impacted by boiling, because this solubility-controlled process can modify only elemental ratios but not isotopic ratios. Assuming a mixing of ASW at 12 °C and injectate and using F(^{84}Kr) values, leads to a injectate contribution of 99.5% and 76.8% for wells AZ-6 and AZ-90, respectively.

In conclusion, it is apparent that the re-injection of used brines (injectate) has begun to significantly affect reservoir fluids at the LAGF. Produced fluids from multiple wells in the LAGF represent pre-production fluids (containing terrigenic argon) diluted by injectate.

6. Conclusions

An expanded noble gas study was conducted in Los Azufres Geothermal Field (LAGF) in Mexico in 2014 following the previous pioneering noble gas study in the LAGF in 2007/2009 (Pinti et al., 2013). Geothermal fluids samples from production wells and hot springs were analyzed for noble gas signatures and strontium isotopes to understand the evolution of fluid circulation following three decades of exploitation and re-injection of used brines.

^{3}He/^{4}He ratios (R), normalized to the atmospheric ratio (Ra = 1.384 × 10^{-6}) range from 3.05 to 7.93 for most samples and point to a binary mixture between a fluid carrying a pure upper mantle helium component and one with helium diluted by atmospheric and/or radiogenic ^{4}He. Crustal He contributes up to 53% and 18% of total He in the NPZ and SPZ, respectively. Comparison between R/Ra and ^{87}Sr/^{86}Sr ratios allows identification of the heat sources in the field. Mantle volatiles (^{3}He) and heat is brought into the LAGF by MORB-like and rhyolitic parental magma bodies intruded within the last 50 kyrs, which provide high enthalpy to the Los Azufres hydrothermal system. In addition to helium, these intrusions also transport heat (Q) into the LAGF reservoir. The observed large range of ^{3}He/Q values in the LAGF fluids suggests that heat has been transferred by both conduction and convection. The heat transfer mechanism appears to be similar in both the NPZ and SPZ.

Atmospheric noble gas isotopic ratios (^{20}Ne/^{36}Ar, ^{84}Kr/^{36}Ar and ^{132}Xe/^{36}Ar) suggest that geothermal wells located closer to the western re-injection zone show a greater contribution of injectate. Overall, it is apparent that the impact of injectate on LAGF reservoir fluids has increased since 2009 and the contribution of injectate with respect to the total Los Azufres geothermal fluids is estimated to be 76.8% and 99.5% for production well AZ-90 (NPZ) and AZ-6 (SPZ), respectively. *Re*-injection activities since 1982 lead to the occurrence of boiling and phase separation at depth in the LAGF reservoir. The boiling zone has further extended to the north and the west since the last noble gas sampling campaign in 2009.

Acknowledgements

This work is funded by CeMieGEO P-20 project from the CONACYT. We wish to thank the *Comission Federal de l'Electricidad* (CFE) de Morelia and Los Azufres for assistance during sampling. DLP is supported by a NSERC Discovery Grant RGPIN-2015-05378. Financial support the NSF Instrumentation & Facilities award EAR-1049822 is greatly appreciated. We wish to thank two anonymous reviewers for their thoughtful comments, which helped improve the manuscript. We thank Dr. David Hilton and Dr. Hailiang Dong for the editorial handling of this manuscript. This work is dedicated to the memory of our late friend and Chemical Geology's editor, David Hilton.

References

Arellano, V.M., Barragán, R.M., Ramírez, M., López, S., Aragón, A., Paredes, A., Casimiro, E., Reyes, L., 2015. Reservoir processes related to exploitation in Los Azufres (Mexico) geothermal field indicated by geochemical and production monitoring data. Int. J. Geosci. 06, 1048–1059. http://dx.doi.org/10.4236/ijg.2015.69083.

Armenta, M.F., Montes, M.R., Leon, H.D.D., 2016. Mexican Geothermal Activities and the New Electricity Market. (CFE Internal Report).

Baker, E.T., Lupton, J.E., 1990. Changes in submarine hydrothermal ^{3}He/heat ratios as an indicator of magmatic/tectonic activity. Nature 346, 556–558. http://dx.doi.org/10.1038/346556a0.

Barragán, R.M., Arellano, V.M., Portugal, E., Sandoval, F., 2005. Isotopic (δ^{18}O, δD) patterns in Los Azufres (Mexico) geothermal fluids related to reservoir exploitation. Geothermics 34, 527–547. http://dx.doi.org/10.1016/j.geothermics.2004.12.006.

Birkle, P., Merkel, B., Portugal, E., Torres-Alvarado, I.S., 2001. The origin of reservoir fluids in the geothermal field of Los Azufres, Mexico — isotopical and hydrological indications. Appl. Geochem. 16, 1595–1610.

Birkle, P., Marín, E.P., Pinti, D.L., Castro, M.C., 2016. Origin and evolution of geothermal fluids from Las Tres Vírgenes and Cerro Prieto fields, Mexico – co-genetic volcanic activity and paleoclimatic constraints. Appl. Geochem. 65, 36–53. http://dx.doi.org/10.1016/j.apgeochem.2015.10.009.

Burnard, P.G., Polya, D.A., 2004. Importance of mantle derived fluids during granite associated hydrothermal circulation: He and Ar isotopes of ore minerals from Panasqueira. Geochim. Cosmochim. Acta 68, 1607–1615. http://dx.doi.org/10.1016/j.gca.2003.10.008.

Burnard, P., Graham, D., Turner, G., 1997. Vesicle-specific noble gas analyses of "popping rock": implications for primordial noble gases in Earth. Science 276, 568–571.

Burnard, P.G., Hu, R.Z., Turner, G., Bi, X.W., 1999. Mantle, crustal and atmospheric noble gases in Ailaoshan gold deposits, Yunnan Province, China. Geochim. Cosmochim. Acta 63 (10), 1595–1604.

Burnard, P., Graham, D., Farley, K., 2004. Fractionation of noble gases (He, Ar) during MORB mantle melting: a case study on the Southeast Indian Ridge. Earth Planet. Sci. Lett. 227, 457–472.

Castro, M.C., Jambon, A., de Marsily, G., Schlosser, P., 1998a. Noble gases as natural tracers of water circulation in the Paris Basin: 1. Measurements and discussion of their origin and mechanisms of vertical transport in the basin. Water Resour. Res. 34, 2443–2466. http://dx.doi.org/10.1029/98WR01956.

Castro, M.C., Goblet, P., Ledoux, E., Violette, S., de Marsily, G., 1998b. Noble gases as natural tracers of water circulation in the Paris Basin. 2. Calibration of a groundwater flow model using noble gas isotope data. Water Resour. Res. 34 (10), 2467–2483.

Castro, M.C., Patriarche, D., Goblet, P., 2005. 2-D numerical simulations of groundwater flow, heat transfer and ^{4}He transport - implications for the he terrestrial budget and the mantle helium-heat imbalance. Earth Planet. Sci. Lett. 237, 893–910. http://dx.doi.org/10.1016/j.epsl.2005.06.037.

Clarke, W.B., Jenkins, W.J., Top, Z., 1976. Determination of tritium by mass spectrometric measurement of ^{3}He. Int. J. Appl. Radiat. Isot. 27, 515–522. http://dx.doi.org/10.1016/0020-708X(76)90082-X.

Condie, K.C., 1993. Chemical composition and evolution of the upper continental crust: contrasting results from surface samples and shales. Chem. Geol. 104, 1–37. http://dx.doi.org/10.1016/0009-2541(93)90140-E.

Craig, H., Lupton, J.E., Welhan, J.A., 1978. Helium isotope ratios in Yellowstone and Lassen Park volcanic gases. Geophys. Res. Lett. 5, 897–900. http://dx.doi.org/10.1029/gl005i011p00897.

Crovetto, R., Fernandez-Prini, R., Japas, M.L., 1982. Solubilities of inert gases and methane in H_2O and in D_2O in the temperature range of 300 to 600 K. J. Chem. Phys. 76, 1077–1086. http://dx.doi.org/10.1063/1.443074.

De la Cruz, V., Aguilar, J., Ortega, D., Sandova, J.M., 1982. Estudio geologico-estructural a detalle del campo geotérmico Los Azufres, Mich. In: CFE Internal Report XX.

Dobson, P.F., Mahood, G.A., 1985. Volcanic stratigraphy of the Los Azufres geothermal area, Mexico. J. Volcanol. Geotherm. Res. 25, 273–287. http://dx.doi.org/10.1016/0377-0273(85)90017-4.

Donnelly, K.E., Goldstein, S.L., Langmuir, C.H., Spiegelman, M., 2004. Origin of enriched ocean ridge basalts and implications for mantle dynamics. Earth Planet. Sci. Lett. 226, 347–366.

Elders, W.A., Bird, D.K., Williams, A.E., Schiffman, P., 1984. Hydrothermal flow regime and magmatic heat source of the Cerro Prieto geothermal system, Baja California, Mexico. Geothermics 13, 27–47.

Ferrari, L., Garduno, V.H., Pasquare, G., Tibaldi, A., 1991. Geology of Los Azufres caldera, Mexico, and its relationships with regional tectonics. J. Volcanol. Geotherm. Res. 47, 129–148.

Flores-Espino, F., Booth, S., Graves, A., 2017. Mexico's Geothermal Market Assessment Report. http://dx.doi.org/10.2172/1349719.

Garcia-Estrada, G., Lopez-Hernandez, A., Prol-Ledesma, R.M., 2001. Temperature–depth relationships based on log data from the Los Azufres geothermal field, Mexico. Geothermics 30 (1), 111–132.

González-Partida, E., Birkle, P., Torres-Alvarado, I.S., 2000. Evolution of the hydrothermal system at Los Azufres, Mexico, based on petrologic, fluid inclusion and

isotopic data. J. Volcanol. Geotherm. Res. 104, 277–296. http://dx.doi.org/10.1016/S0377-0273(00)00211-0.
González-Partida, E., Carrillo-Chávez, A., Levresse, G., Tello-Hinojosa, E., Venegas-Salgado, S., Ramirez-Silva, G., Pal-Verma, M., Tritlla, J., Camprubi, A., 2005. Hydrogeochemical and isotopic fluid evolution of the Los Azufres geothermal field, Central Mexico. Appl. Geochem. 20, 23–39. http://dx.doi.org/10.1016/j.apgeochem.2004.07.006.
Graham, D.W., 2002. Noble gas isotope geochemistry of Mid-Ocean ridge and Ocean Island basalts: characterization of mantle source reservoirs. Rev. Mineral. Geochem. 47, 247–317. http://dx.doi.org/10.2138/rmg.2002.47.8.
Hayba, D.O., Ingebritsen, S.E., 1997. Multiphase groundwater flow near cooling plutons. J. Geophys. Res. Planets 102, 12235–12252. http://dx.doi.org/10.1029/97JB00552.
Hilton, D.R., Porcelli, D., 2003. 2.06 - noble gases as mantle tracers. In: Turekian, H.D.H.K. (Ed.), Treatise on Geochemistry. Pergamon, Oxford, pp. 277–318. http://dx.doi.org/10.1016/B0-08-043751-6/02007-7.
Hilton, D.R., Hammerschmidt, K., Loock, G., Friedrichsen, H., 1993a. Helium and argon isotope systematics of the central Lau Basin and Valu Fa Ridge: evidence of crust/mantle interactions in a back-arc basin. Geochim. Cosmochim. Acta 57, 2819–2841. http://dx.doi.org/10.1016/0016-7037(93)90392-A.
Hilton, D.R., Hammerschmidt, K., Teufel, S., Friedrichsen, H., 1993b. Helium isotope characteristics of Andean geothermal fluids and lavas. Earth Planet. Sci. Lett. 120, 265–282. http://dx.doi.org/10.1016/0012-821X(93)90244-4.
Kelemen, P.B., Hanghoj, K., Greene, A.R., 2004. One view of the geochemistry of subduction-related magmatic arcs, with an emphasis on primitive andesite and lower crust. In: Holland, H.D., Turekian, K.K. (Eds.), Treatise on Geochemistry. 3. Elsevier, Amsterdam, pp. 593–659.
Kennedy, B.M., 1988. Noble gases in vent water from the Juan de Fuca Ridge. Geochim. Cosmochim. Acta 52, 1929–1935. http://dx.doi.org/10.1016/0016-7037(88)90016-6.
Kennedy, B.M., van Soest, M.C., 2006. A helium isotope perspective on the Dixie Valley, Nevada, hydrothermal system. Geothermics 35 (1), 26–43.
Kennedy, B.M., Lynch, M.A., Reynolds, J.H., Smith, S.P., 1985. Intensive sampling of noble gases in fluids at Yellowstone: I. Early overview of the data; regional patterns. Geochim. Cosmochim. Acta 49, 1251–1261. http://dx.doi.org/10.1016/0016-7037(85)90014-6.
Kennedy, B.M., Hiyagon, H., Reynolds, J.H., 1991. Noble gases from Honduras geothermal sites. J. Volcanol. Geotherm. Res. 45, 29–39.
Kennedy, B.M., Fischer, T.P., Shuster, D.L., 2000. Heat and helium in geothermal systems. In: Proc. 45st Workshop Geother. Res. Engin. Stanford University, Stanford, California (SGP-TR-165).
Lund, J.W., Rangel, M.A., 1995. Pilot fruit drier for the Los Azufres geothermal field, Mexico. In: Processing of The World Geothermal Congress, pp. 2335–2338.
Lupton, J.E., Baker, E.T., Massoth, G.J., Thomson, R.E., Burd, B.J., Butterfield, D.A., Embley, R.W., Cannon, G.A., 1995. Variations in water-column ^{3}He/heat ratios associated with the 1993 CoAxial event, Juan de Fuca Ridge. Geophys. Res. Lett. 22, 155–158. http://dx.doi.org/10.1029/94GL02797.
Martel, D.J., Deak, J., Dövenyi, P., Horvath, F., O'nions, R.K., Oxburgh, E.R., Stegena, L., Stute, M., 1989. Leakage of helium from the Pannonian basin. Nature 342, 908–912. http://dx.doi.org/10.1038/342908a0.
Mazor, E., Bosch, A., 1987. Noble gases in formation fluids from deep sedimentary basins: a review. Appl. Geochem. 2, 621–627. http://dx.doi.org/10.1016/0883-2927(87)90014-X.
Mazor, E., Truesdell, A.H., 1984. Dynamics of a geothermal field traced by noble gases: Cerro Prieto, Mexico. Geothermics 13, 91–102. http://dx.doi.org/10.1016/0375-6505(84)90009-9.
Molina Martínez, A.I.I.I., 2013. Case history of Los Azufres – conceptual modelling in a Mexican geothermal field. In: Short Course V on Conceptual Modelling of Geothermal Systems. UNU-GTP and LaGeo, Santa Tecla, El Salvador, pp. 1–13.
Moreira, M., Kunz, J., Allegre, C., 1998. Rare gas systematics in popping rocks: isotopic and elemental compositions in the upper mantle. Science 279, 1178–1180.
Morikawa, N., Kazahaya, k., Masuda, H., Ohwada, M., Nakama, A., Nagao, K., Sumino, H., 2008. Relationship between geological structure and helium isotopes in deep ground-water from the Osaka Basin: application to deep groundwater hydrology. Geochem. J. 42, 61–74. http://dx.doi.org/10.2343/geochemj.42.61.
Oxburgh, E.R., O'nions, R.K., Hill, R.I., 1986. Helium isotopes in sedimentary basins. Nature 324, 632–635. http://dx.doi.org/10.1038/324632a0.
Ozima, M., Podosek, F.A., 1983. Noble Gas Geochemistry. Cambridge University Press, Cambridge.
Paonita, A., Caracausi, A., Iacono-Marziano, G., Martelli, M., Rizzo, A., 2012. Geochemical evidence for mixing between fluids exsolved at different depths in the magmatic system of Mt Etna (Italy). Geochim. Cosmochim. Acta 84, 380–394. http://dx.doi.org/10.1016/j.gca.2012.01.028.
Phillips, D.L., Koch, P.L., 2002. Incorporating concentration dependence in stable isotope mixing models. Oecologia 130, 114–125.
Pinti, D.L., Marty, B., 1995. Noble gases in crude oils from the Paris Basin, France: implications for the origin of fluids and constraints on oil-water-gas interactions. Geochim. Cosmochim. Acta 59, 3389–3404. http://dx.doi.org/10.1016/0016-7037(95)00213-J.
Pinti, D.L., Castro, M.C., Shouakar-Stash, O., Tremblay, A., Garduño, V.H., Hall, C.M., Hélie, J.F., Ghaleb, B., 2013. Evolution of the geothermal fluids at Los Azufres, Mexico, as traced by noble gas isotopes, δ^{18}O, δD, δ^{13}C and ^{87}Sr/^{86}Sr. J. Volcanol. Geotherm. Res. 1–11. http://dx.doi.org/10.1016/j.jvolgeores.2012.09.006.
Pinti, D.L., Castro, M.C., Lopez-Hernandez, A., Han, G., Shouakar- Stash, O., Hall, C.M., Ramírez-Montes, M., 2017. Fluid circulation and reservoir conditions of the Los Humeros Geothermal Field (LHGF), Mexico, as revealed by a noble gas survey. J. Volcanol. Geotherm. Res. http://dx.doi.org/10.1016/j.jvolgeores.2017.01.015.
Pradal, E., Robin, C., 1994. Long-lived magmatic phases at Los Azufres volcanic center, Mexico. J. Volcanol. Geotherm. Res. 63, 201–215. http://dx.doi.org/10.1016/0377-0273(94)90074-4.
Saar, M.O., Castro, M.C., Hall, C.M., Manga, M., Rose, T.P., 2005. Quantifying magmatic, crustal, and atmospheric helium contributions to volcanic aquifers using all stable noble gases: implications for magmatism and groundwater flow. Geochem. Geophys. Geosyst. 6, Q03008. http://dx.doi.org/10.1029/2004GC000828.
Salters, V.J.M., Stracke, A., 2004. Composition of the depleted mantle. Geochem. Geophys. Geosyst. 5. http://dx.doi.org/10.1029/2003GC000597.
Sano, Y., Fischer, T.P., 2013. The analysis and interpretation of noble gases in modern hydrothermal systems. In: Burnard, P. (Ed.), The Noble Gases as Geochemical Tracers. Springer Berlin Heidelberg, Berlin, Heidelberg, pp. 249–317.
Sano, Y., Takahata, N., Seno, T., 2006. Geographical distribution of ^{3}He/^{4}He ratios in the Chugoku District, southwestern Japan. In: Paragenesis of Fluids Under Evaporates in the Volga-Ural Basin. 163. pp. 745–757. http://dx.doi.org/10.1007/s00024-006-0035-0.
Sarda, P., Staudacher, T., Allègre, C.J., 1988. Neon isotopes in submarine basalts. Earth Planet. Sci. Lett. 91, 73–88.
Segovia, N., Barragán, R.M., Tello, E., 2005. Geochemical characteristics and ^{222}Rn measurements at Cuitzeo Basin (Mexico) thermal springs and artesian wells. In: Proc World Geothermal Congress.
Smith, S.P., 1985. Noble gas solubility in water at high temperature. Eos 66, 397.
Smith, S.P., Kennedy, B.M., 1983. The solubility of noble gases in water and in NaCl brine. Geochim. Cosmochim. Acta 47, 503–515. http://dx.doi.org/10.1016/0016-7037(83)90273-9.
Smith, S.P., Kennedy, B.M., 1985. Noble gas evidence for two fluids in the Baca (Valles Caldera) geothermal reservoir. Geochim. Cosmochim. Acta 49, 893–902.
Staudacher, T., Sarda, P., Richardson, S.H., Allègre, C.J., Sagna, I., Dmitriev, L.V., 1989. Noble gases in basalt glasses from a Mid-Atlantic Ridge topographic high at 14°N: geodynamic consequences. Earth Planet. Sci. Lett. 96, 119–133.
Stuart, F.M., Burnard, P.G., Taylor, R.P., Turner, G., 1995. Resolving mantle and crustal contributions to ancient hydrothermal fluids: He–Ar isotopes in fluid inclusions from Dae Hwa W–Mo mineralisation, South Korea. Geochim. Cosmochim. Acta 59, 4663–4673.
Torgersen, T., Habermehl, M.A., Clarke, W.B., 1992. Crustal helium fluxes and heat flow in the Great Artesian Basin, Australia. Chem. Geol. 102, 139–152. http://dx.doi.org/10.1016/0009-2541(92)90152-U.
Torres-Rodriguez, M.A., Mendoza-Covarrubias, A., Medina-Martinez, M., 2005. An Update of the Los Azufres Geothermal Field, After 21 Years of Exploitation. pp. 1–8.
Turner, G., Stuart, F., 1992. Helium/heat ratios and deposition temperatures of sulphides from the ocean floor. Nature 357, 581–583. http://dx.doi.org/10.1038/357581a0.
Verma, S.P., Torres-Alvarado, I.S., Satir, M., Dobson, P.F., 2005. Hydrothermal alteration effects in geochemistry and Sr, Nd, Pb, and O isotopes of magmas from the Los Azufres geothermal field (Mexico): a statistical approach. Geochem. J. 39, 141–163. http://dx.doi.org/10.2343/geochemj.39.141.
Viggiano-Guerra, J.C., Gutiérrez-Negrín, L.C.A., 2005. The geothermal system of Araró, Mexico, as an independent system of Los Azufres. In: Proc. World Geother. Congr., Antalya, Turkey, pp. 1–6.
Wen, T., Castro, M.C., Ellis, B.R., Hall, C.M., Lohmann, K.C., 2015a. Assessing compositional variability and migration of natural gas in the Antrim Shale in the Michigan Basin using noble gas geochemistry. Chem. Geol. 417, 356–370. http://dx.doi.org/10.1016/j.chemgeo.2015.10.029.
Wen, T., Castro, M.C., Hall, C.M., Pinti, D.L., Lohmann, K.C., 2015b. Constraining groundwater flow in the glacial drift and saginaw aquifers in the Michigan Basin through helium concentrations and isotopic ratios. Geofluids 16, 3–25. http://dx.doi.org/10.1111/gfl.12133.
Wen, T., Castro, M.C., Nicot, J.-P., Hall, C.M., Larson, T., Mickler, P., Darvari, R., 2016. Methane sources and migration mechanisms in shallow groundwaters in Parker and Hood counties, Texas—a heavy noble gas analysis. Environ. Sci. Technol. 50, 12012–12021. http://dx.doi.org/10.1021/acs.est.6b01494.
Wen, T., Castro, M.C., Nicot, J.P., Hall, C.M., Pinti, D.L., Mickler, P., Darvari, R., Larson, T., 2017. Characterizing the noble gas isotopic composition of the Barnett Shale and Strawn group and constraining the source of stray gas in the Trinity Aquifer, north-central Texas. Environ. Sci. Technol. 51 (11), 6533–6541.